

Galaxy morphology, kinematics and clustering in a hydrodynamic simulation of a Λ CDM universe

Rupert A.C. Croft^{1,2*}, Tiziana Di Matteo^{1,2}, Volker Springel³ and Lars Hernquist⁴

¹ *Dept. of Physics, Carnegie Mellon University, Pittsburgh, PA 15213, USA*

² *Bruce and Astrid McWilliams Center for Cosmology, Carnegie Mellon University, Pittsburgh, PA 15213, USA*

³ *Max Planck Institute for Astrophysics, 85741 Garching, Germany*

⁴ *Harvard-Smithsonian Center for Astrophysics, 60 Garden Street, Cambridge, MA 02138, USA*

29 October 2018

ABSTRACT

We explore galaxy properties and their link with environment and clustering using a population of ~ 1000 galaxies formed in a high resolution hydrodynamic simulation of the Λ CDM cosmology. At the redshift we concentrate on, $z = 1$, the spatial resolution is 1.4 proper h^{-1} kpc and the mass resolution is such that Milky-way sized disk galaxies contain $\sim 10^5$ particles within their virial radii. The simulations include supermassive black hole accretion and feedback as well as a multiphase model for star formation. Overall, we find that a number of familiar qualitative relationships hold approximately between galaxy properties, for example we observe galaxies as lying between two broad extremes of type, where “late” types tend to be smaller in size, have lower circular velocities, younger stars, higher star formation rates, larger disk to bulge ratios and lower Sersic indices than “early types”. We find that as in previous studies of small numbers of resimulated galaxies the stellar component of disk galaxies is not as rotationally supported as in observations. Bulges contain too much of the stellar mass, although exponential disks do have scale lengths compatible with observations, and the stellar mass Tully-Fisher relation at $z = 1$ is reproduced. The addition of black hole physics to the simulations does not appear to have made a large impact on the angular momentum results compared to these other studies, nor do we find that running an identical simulation with significantly lower mass resolution affects this aspect. Despite this, we can profitably use the rank order of either disk to total ratio, Sersic index, or galaxy age to separate galaxies into morphological classes and examine the density-morphology relation and morphology dependence of clustering. We find that while at redshift $z = 0$, the well known preponderance of early types in dense environments is seen, at $z = 1$ the density-morphology relation becomes flatter and late type galaxies are even seen to have a higher clustering amplitude than early types.

Key words: Cosmology: observations – Galaxies, large-scale structure of Universe

1 INTRODUCTION

Forming realistic galaxies is one of the grand challenges for numerical cosmology. A promising approach assumes that this can be done, given the correct cosmological model and enough spatial and mass resolution in a simulation of the physics of gravitational collapse of gas and dark matter, Pioneering work in this vein (e.g., Evrard 1988, Hernquist & Katz 1989) included some of the physical implementations (Smoothed Particle Hydrodynamics, Gingold & Monaghan,

1977, Lucy 1977) still most used today. Gradual improvements and additions, including star formation (e.g. Katz 1992), feedback (e.g., Springel and Hernquist 2003a), black hole accretion (e.g., Di Matteo et al. 2005, Springel et al. 2005, Okamoto et al. 2007) have led to better modelling of galaxy properties (e.g., Abadi et al. 2003a,b, Governato et al. 2007). The most striking result to come from this research effort is the generic problem of too little angular momentum and too centrally concentrated galaxies (see e.g., the recent review by Mayer et al. 2008). Many aspects of our understanding of galaxy formation have been progressing, however, spurred on by high resolution “zoomed” resimula-

* E-mail: rcroft@cmu.edu

tions of individual galaxies (e.g. Abadi et al. 2003, Sommer-Larsen et al. 2003, Governato et al. 2004, Robertson et al. 2004, Zavala et al. 2007) In the meantime, larger-scale simulations (e.g., Springel et al. 2005, Weinberg et al. 2004) have led to better predictions of the large scale clustering properties of galaxies. In the present paper, we aim to address questions which link both approaches, by looking at internal properties of galaxies which form in a cosmological volume with uniformly high resolution. In this way we can look at not only the properties of a wide range of galaxies, but the relation of these properties with their large scale environments.

Using the same simulation to study individual galaxies and the evolution of structure in a cosmological volume is necessary to ensure that we deal with a fair sample of galaxies. In zoomed resimulations (e.g., Katz et al. 1994, Robertson et al. 2005) galaxies that are chosen to be followed at high resolution (usually systems relatively free of major mergers at late types) may be special by virtue of their selection, and it is not easy to quantify biases that this may induce in statistical studies of their properties. Running a cosmological volume with enough resolution to carry this out to redshift $z = 0$ is extremely expensive computationally. Motivated both by this and the rapid growth of observational data available for redshift $z = 1$, (e.g., the DEEP2 study of galaxy properties and environment at $z \sim 1$, Cooper et al. 2007, the VVDS survey, Meneux et al. 2008, and COMBO-17 survey, Bell et al. 2004) we focus most of our attention on a large, high resolution simulation run to this redshift. Results from this computation, known as the *BHCosmo* run were first presented by Di Matteo et al. (2007). It features the first direct inclusion of supermassive black hole accretion and feedback in a cosmological hydrodynamic model.

The questions which can be asked include whether we are able to make disk galaxies which look like observed spirals, and whether they lie on the Tully-Fisher relation. Having a large statistical sample of simulated galaxies will enable studies of how their properties are correlated and interrelated, for example how disk scales lengths are related to circular velocities and so on. In the present study we do not carry out population synthesis modelling, instead concentrating on morphology of stellar mass density, stellar and gas kinematics and other related measures of galactic structure.

Observationally, large datasets of galaxies at redshifts $z \gtrsim 1$ are becoming available. As mentioned above, with the DEEP2 redshift survey (see e.g., Coil et al. 2008 and references therein) data it has become possible to look at the dependence of galaxy clustering on color, luminosity and other properties. HST images of galaxies with enough resolution for morphological classification have extended studies of the morphology-density relation to $z \sim 0.5 - 1.0$ (see e.g., the early work of the MORPHS collaboration, Dressler et al. 1997 through Smith et al. 2005). At higher redshifts, Peter et al. (2007) have also measured galaxy morphologies in the environment of a rich cluster at redshift $z = 2.3$ using HST/ACS images. With the increase in observational data available at these redshifts, it is important to investigate the robustness of theoretical modelling with a variety of techniques. For example, Zheng et al. (2007) have fit Halo Occupation Distribution models to the luminosity dependence of clustering in DEEP2 and Croton et al. (2006)

have made semi-analytic model predictions for the clustering strengths of red and blue galaxies at redshifts relevant for DEEP2. In the present work, we explore the predictions of hydrodynamic simulations.

Our plan for this paper is as follows. In Section 2 we describe the cosmological simulations, how we select galaxies from the simulation outputs and show some images of examples of late and early type galaxies. In Section 3 we investigate galaxy properties in detail, including kinematically defined bulge to disk ratios, and projected stellar density profiles. We show how measurements of these quantities are affected by simulation resolution and then examine the relationships between all the properties for individual galaxies. We also plot the angular momentum content of late type galaxies and compare it to observations, as well as comparing to the observed stellar mass Tully-Fisher relation. In Section 4 we focus on the relationship between galaxy properties and environment, including comparison to the observed density morphology relation. In Section 5 we look at large scale structure in the simulated galaxy distribution and compute the autocorrelation function. We summarize and discuss our findings in Section 6.

2 SIMULATION

We have carried out a large cosmological simulation, using the SPH code Gadget-2 (Springel 2005), with the inclusion of modelling of black hole accretion and feedback, previously used in simulations of isolated galaxies and galaxy mergers (Di Matteo et al. 2005, Springel et al. 2005). This direct cosmological simulation of black hole evolution in a cosmological context, known as the *BHCosmo* simulation is presented and described in more detail in Di Matteo et al. (2007). The simulation algorithms and description of the black hole population that forms and its relationship to galaxies in the simulation are also set out in that paper. A slightly different approach to modelling black holes in cosmological Gadget-2 simulations, including feedback from a “radio mode” is also presented by Sijacki et al. (2007). Okamoto et al. (2007) have also incorporated their own modelling of black hole physics in zoomed simulations (also run with Gadget-2) of individual galaxies. We discuss some similarities with our results in Section 6.2

Besides black hole feedback, the simulation includes the multiphase star formation model of Springel & Hernquist (2003a), in which stellar wind particles can propagate from the sites of star formation and carry energy over large distances. This model was previously used in the zoomed simulation of an individual disk galaxy in a cosmological context by Robertson et al. (2005).

The cosmological parameters used as inputs to the *BHCosmo* simulation are consistent with the WMAP first year results (Spergel et al. 2003), i.e. $h = 0.7 = H_0/100 \text{ km s}^{-1} \text{ Mpc}^{-1}$, matter content $\Omega_m = 0.3$, cosmological constant $\Omega_\Lambda = 0.7$, baryon content $\Omega_b = 0.04$ and amplitude of mass fluctuations, $\sigma_8 = 0.9$. The simulation volume is a periodic cube of side length $33.75 h^{-1} \text{ Mpc}$, and the *BHCosmo* contains 486^3 dark matter and initially 486^3 gas particles, giving a mass resolution of $2.75 \times 10^7 h^{-1} \text{ M}_\odot$ per dark matter particle and $4.24 \times 10^6 h^{-1} \text{ M}_\odot$ per gas particle. We evolve the simulation from redshift $z = 99$ down to $z = 1$, using con-

stant gravitational softening in comoving units. At $z = 1$, the force resolution is 1.4 proper h^{-1} kpc.

The *BHCosmo* simulation has a mass and force resolution that fits into the scheme devised by Springel & Hernquist (2003b), who ran a set of simulations with box size varying by factors of ~ 3 and particle numbers by factors of 1.5^3 . In their naming scheme, the *BHCosmo* would be equivalent to a D6 simulation. We have also run another simulation with the same initial conditions, box size and physical modelling but coarser mass and force resolution (equivalent to D4, i.e. 2×216^3 particles). We use this D4 run, which has a mass per particle 11.4 times greater than the *BHcosmo*, and force resolution 2.3 times larger, to gauge the effects of resolution on our results, as was done by Di Matteo et al. (2007). Because the D4 was run with the same random initial Fourier phases as the *BHcosmo* it is possible to identify the same objects which form in both runs and therefore make direct comparisons (we shall do this in §3.3).

2.1 Galaxy selection

We select galaxies from the particle distributions using a variant of the subgroup finder SUBFIND (see Springel et al. 2001). This selects gravitationally bound clumps of particles, using the gas, dark matter and stellar content of groups to do this. Each subgroup is therefore deemed to be an individual galaxy. Each galaxy is also associated with a friends-of-friends group, which is found using the usual method, linking together particles connected by less than 0.2 times the mean interparticle separation. Particles within the friends-of-friends group are approximately those that lie within the virial overdensity threshold of a dark matter halo.

From the list of galaxies, we pick those which have more than 5000 particles in the *BHCosmo* run, in order to limit the noise on morphological and kinematic properties measured from the galaxy particle distributions. At $z = 1$, we have 1180 galaxies in the *BHCosmo* simulation. The particle number cut is essentially equivalent to a cut in circular velocity of 100 km s^{-1} . We find that at $z = 1$, galaxies of similar mass to the Milky Way (those with circular velocities within 10% of 220 km s^{-1}) contain ~ 60000 particles on average. For the D4 low resolution run we use an appropriately lower threshold on the particle number (439 particles).

For each galaxy (i.e. subgroup) we define a central point, which is the particle (star, gas or dark matter) at the minimum of the gravitational potential. This particle serves as a center when computing the stellar density and angular momentum profiles and for all other purposes in the paper when the center of the galaxy is required.

2.2 Example galaxies

Before characterizing the statistical properties of our sample of galaxies, we examine their morphology visually. To do this, we take galaxies from the redshift $z = 1$ output of the *BHCosmo* run. In Figures 1 and 2, we show 10 representative galaxies taken from two classes, those with high D/T (Disk to Total) ratios and low D/T ratios respectively. The D/T ratio is derived from a kinematic decomposition of the stellar mass content of each galaxy (following e.g., Abadi et al. 2003a), and will be more fully explored in §3.1 For now it is

sufficient to state that these decompositions form the basis for one possible separation into “late” type disk galaxies and “early” type ellipticals.

Figure 1 shows galaxies that lie principally in the top 10% or so of D/T values, although because most galaxies are bulge dominated, even these include some with D/T values less than 0.5. We note that zoomed resimulations of disk galaxies in other work typically have similar D/T ratios (see e.g., Abadi et al. 2003b in which the galaxy had D/B of 0.83, or D/T of 0.45). The plot shows two views each of the stellar density, gas density and dark matter density, on a logarithmic scale. If the angular momentum vector of the stellar component defines the z -axis, the two panels for each component show the face on ($x-y$) view and a side on ($x-z$) view. We can see that the stellar components are flattened in the direction expected if they are rotationally supported. They are not particularly thin, and an obvious bulge is not easy to spot in the surface brightness plots. Comparing with the zoomed simulations of disk galaxies performed by Robertson et al. 2004 (their figure 3, top left) or Governato et al. 2007 (their figure 6, left panels), we can see similar morphologies.

The gas components in Figure 1 are more varied in appearance than the stars, with most galaxies having relatively thin disks. Some however (such as the second and third from bottom) have rather clumpy distributions and are less obviously flat. Approximately half the dark matter halos can be seen to be obviously slightly flattened in the same direction as the stellar disks. Alongside the plots, we have listed the D/T ratios and the total mass of the subhalo. Most of the disk galaxies we plot are fairly large, with total mass around $10^{12} h^{-1} M_{\odot}$. The fifth from the top, the largest and most massive has the lowest D/T ratio. We also show next to each panel an indicator of the physical size of the galaxy, the radius of a sphere which encloses half the stellar mass (r_{half}), in proper h^{-1} kpc.

Moving to the early types in Figure 2, one immediate difference that can be seen from the stellar density plots is that they do appear to be more centrally concentrated than the disks. On average, the ratio of major to minor axes appears to be lower, and the orientation of the galaxy also appears to have little relation to the angular momentum direction (as expected, given that these galaxies were selected on the basis of their stellar kinematics). The gas components are almost all rather clumpy and roughly spherically distributed, although the first galaxy plotted has a very obvious thin gas disk. This is rather unusual, given the almost spherical nature of its stellar distribution, although we note that it does have the highest D/T ratio of all the galaxies in this plot. Interestingly, the dark matter contours do not appear to be oriented in the same way as the stellar distribution, as any visible degree of correlation between the major axes of the dark matter and stars is hard to pick up on. The gas distributions do appear perhaps to line up slightly better with the dark matter. We have however computed the median angular difference between the directions of the principal axes of the stars and gas (we return to this in §3.7 below) and find a value of 24° , a fairly strong alignment. This value is for all galaxies though, and presumably strongly influenced by the good alignments of gas and stellar disks.

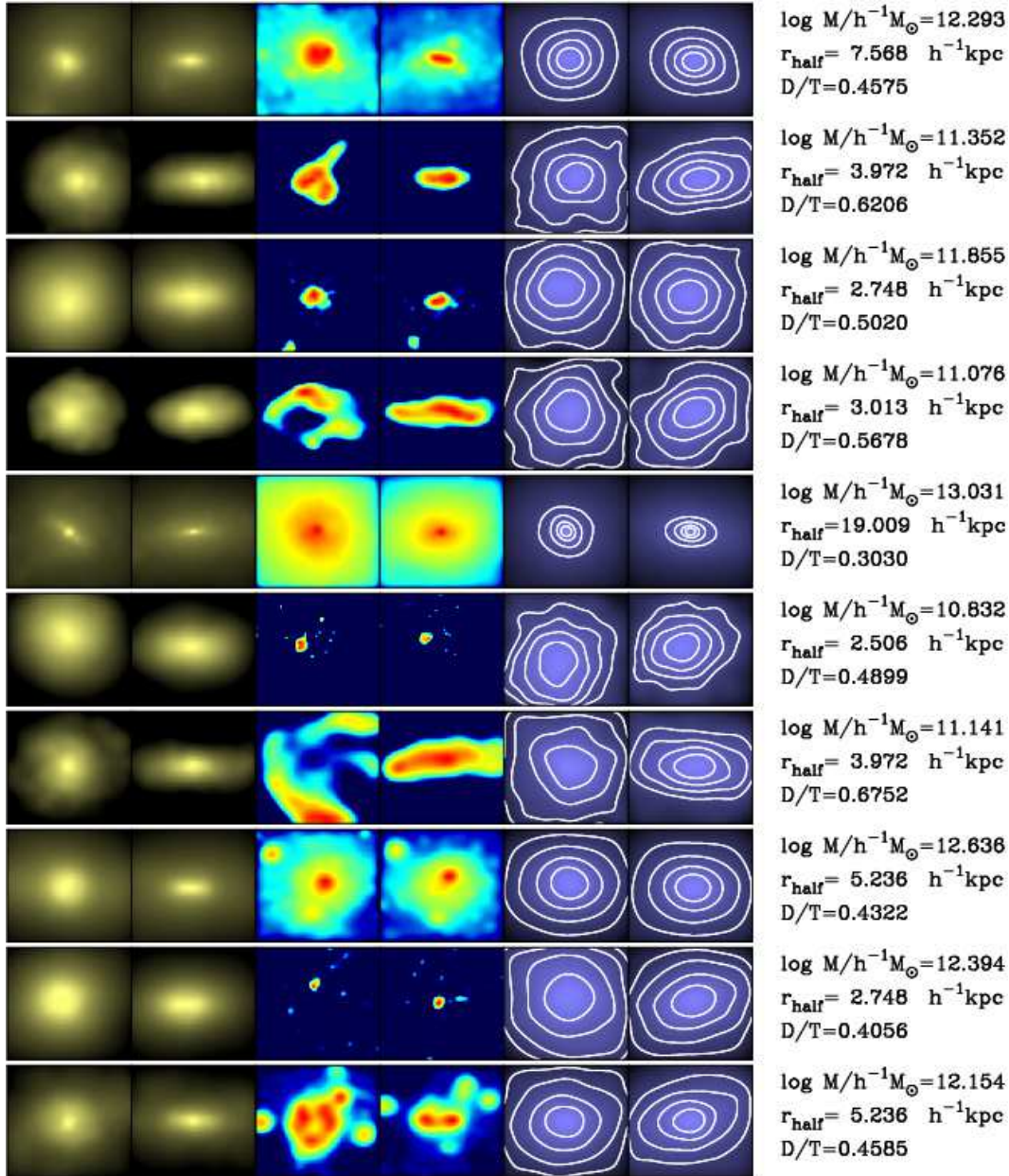


Figure 1. Images of $z = 1$ galaxies from the *BHCosmo* simulation selected kinematically to have a high D/T ratio (i.e., “late types”, see text §3.1). We show 10 galaxies, in no particular order, from the top to the bottom of the page. The three columns with different appearances are from left to right the stellar surface density, the gas surface density and the dark matter surface density in a cube centered on the minimum of the gravitational potential for the galaxy (see §2.1). In each column, there are two panels corresponding to two projections, the leftmost is such that the galaxy is face on, using the angular momentum vector of the star particles in the galaxy to define the direction. The rightmost panel is an edge on projection. All surface densities are plotted with a logarithmic scale, and the contours in the dark matter plots are shown at intervals of 0.2 dex. The length scales are such that each panel shows a region of space from $-2r_{\text{half}}$ to $+2r_{\text{half}}$, where r_{half} is the radius which encloses half the stellar mass. The values of r_{half} for each galaxy (in proper $h^{-1}\text{kpc}$) are shown to the right, along with the D/T ratio and total mass of the galaxy/subgroup (including stars, gas and dark matter.)

3 GALAXY PROPERTIES

We will focus on three main properties of our simulated galaxy sample, their kinematics (angular momentum and kinematic decomposition into disk and bulge), their profiles (quantified by a Sersic index) and their mean stellar ages and star formation rates. We do not classify their morphology by eye as has been done observationally (e.g., by the MORPHIS

group, Dressler et al. 1997), but we will use the kinematic decomposition and Sersic indices as indicators of morphology, for example when investigating the morphology-density relation. We make use of our two simulations, the *BHCosmo* run and the D4 run which have identical initial conditions but different mass and spatial resolution to investigate the effects of biases in galaxy properties due to numerical effects.

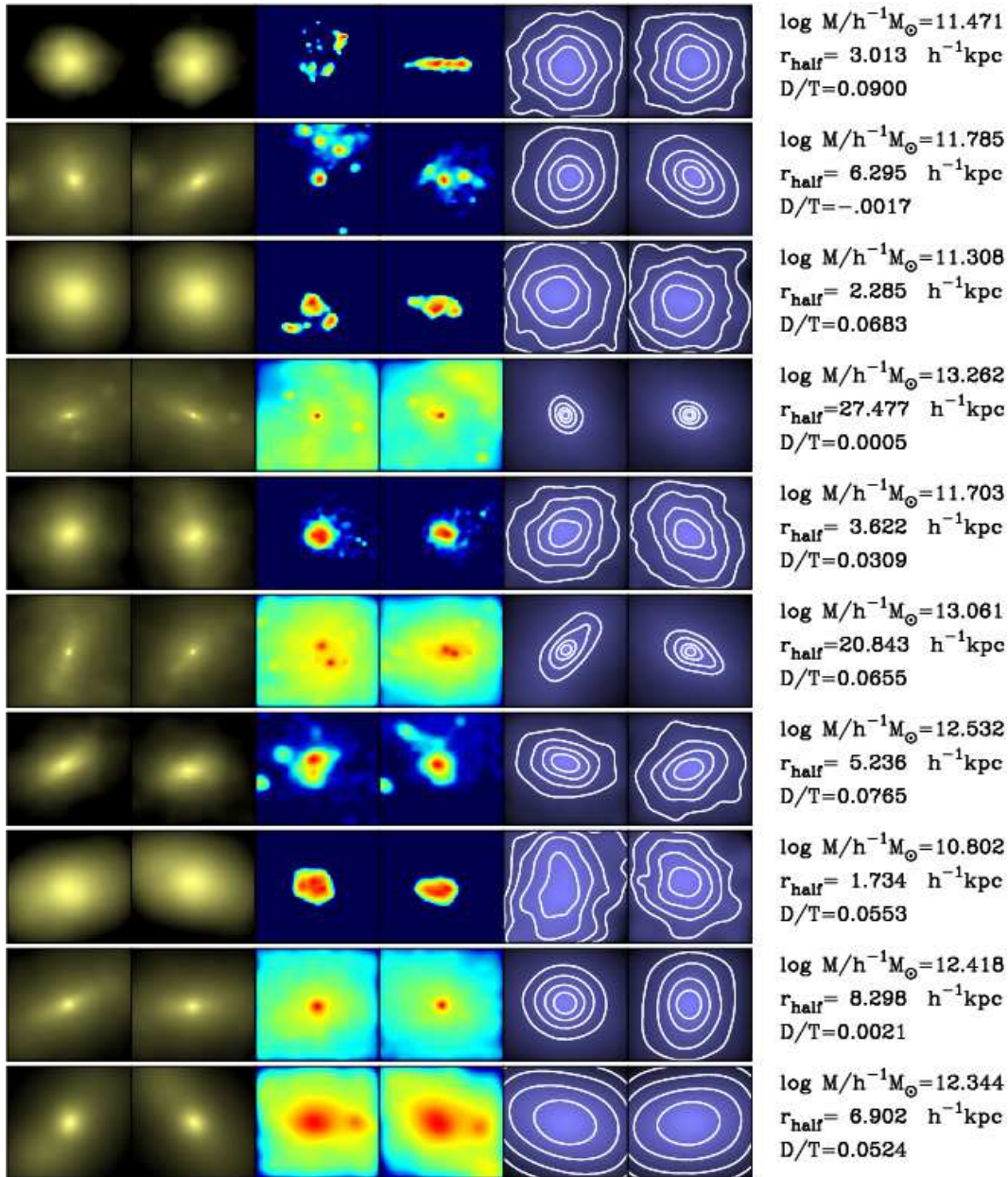


Figure 2. Images of ten $z = 1$ galaxies from the *BHCosmo* simulation selected kinematically to have a low D/T ratio (i.e., “early types”, see text §3.1). We show the stellar, gas and dark matter surface density from left to right, in the same fashion as the late type galaxies in Figure 1.

Comparisons of both simulations are presented in detail in §3.3 below, including some quantification of the effects of resolution. We first explain the measures of kinematics and stellar profiles, also including examples drawn from both simulations.

3.1 Kinematics and D/T ratios

We examine the stellar orbits in the galaxies, following a technique often used in the literature (e.g., Abadi et al. 2003b), we use the angular momenta of individual stars to dynamically decompose the galaxies into disks and spheroids.

In the disk galaxies (Figure 1), the total angular mo-

mentum vector of the stars defines a direction which is visually perpendicular to the stellar disk. We will investigate how well this holds quantitatively later (§3.7), but for now we use this direction to define the z -axis. For a star particle, we compute the specific angular momentum in the z direction, J and also its specific binding energy E . Following exactly the procedure of Abadi et al. (2003b), we compute E relative to the total mass of the galaxy within the viral radius, r_{200} . For each star particle we then compute the specific angular momentum of the corotating circular orbit with the same binding energy, J_c . The ratio J/J_c gives for each particle a measure of the orbital circularity. The maximum value, $J/J_c = 1$ occurs for particles which are following in circular orbits in the same direction as the majority of the

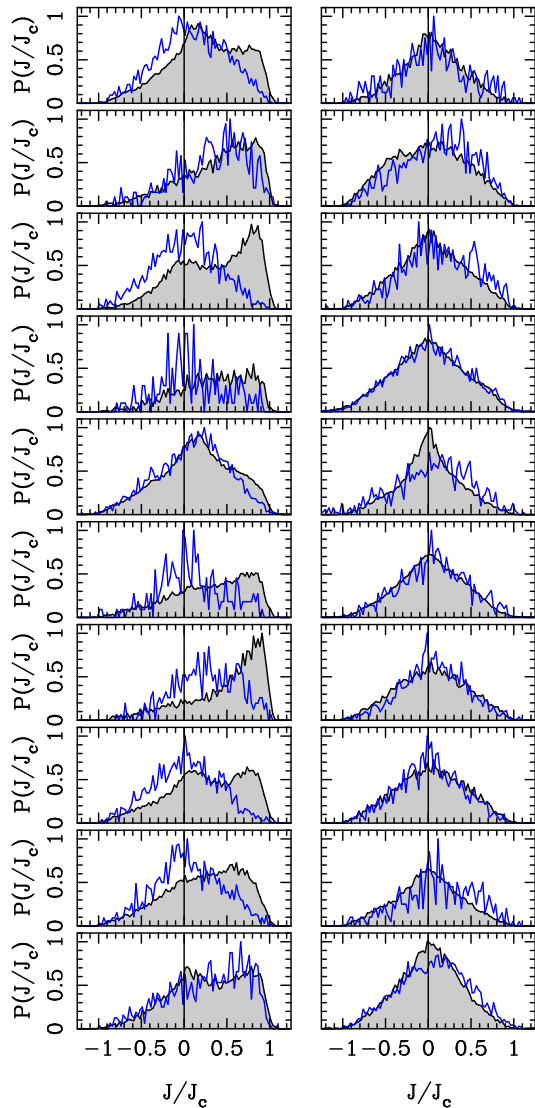


Figure 3. Histograms of the orbital circularity of star particles, J/J_c for the galaxies (at $z = 1$) shown in Figures 1 (late types, left column) and 2 (early types, right column). The quantity J/J_c is the ratio of the orbital angular momentum of an individual star particle to one with the same energy but on a circular orbit (see text). The shaded histograms are for galaxies selected from the *BHCosmo* simulation and the superimposed lines are the same galaxies taken from the lower resolution simulation, D4. How the matching galaxies were found in the D4 run is described in §3.2. The y -axis in each case is the relative probability density, normalized to 1 at the maximum value.

stars. Particles with close to this value are therefore likely to be in a disk component.

In Figure 3, we show histograms of the J/J_c values for all stars for our 20 example galaxies, with the late types on the left, and early types on the right. In order to avoid going out very far into the outskirts of the galaxy where particle numbers are sparse, we only plot particles which lie within 4 half stellar mass radii (r_{half}) of the center of the galaxy (the results are insensitive to this choice). To compute the D/T ratio, we make the (somewhat arbitrary) assumption that the bulge has zero total angular momentum (see e.g., van den Bosch et al. 2002). Starting from the negative end of

the J/J_c distribution we associate all the star particles with negative J/J_c with the bulge as well as an equal mass of star particles with the equivalent positive J/J_c values. The star particles left over then make up the disk. In this way, we compute the disk to total ratio, D/T already enumerated next to the galaxy plots in Figures 1 and 2.

Because the bulge/disk decomposition relies on this J/J_c distribution it is not surprising that the galaxies in the left panel, chosen to be more disk-like have asymmetric histograms. Eight of the ten disk galaxies have the highest point in the J/J_c distribution associated with the region around $J/J_c = 1$, showing that the galaxies indeed have a strong stellar rotationally supported component, as we would expect from their morphology. Some of the distributions are markedly more asymmetric than others, with 2 not showing any real evidence for a spheroid component (a bump centered on $J/J_c = 0$). The shaded histogram is the result for our high resolution *BHCosmo* simulation, and the (somewhat noisier) line is the result for the same galaxies taken from the low resolution D4 model (see Section 3.3 for details on the matching of galaxies in the simulations). We can see that the two simulations can give rather different results for the J/J_c distribution for the same galaxy. This is likely to be due among other things to stochasticity coming from initial fluctuation power below the Nyquist limit of the lower resolution model, and differences in the numerical integration of particle orbits coming from resolution effects. This will lead to a scatter in D/T values between the two simulations. We investigate quantitatively the effect of resolution on this parameter below.

The low D/T galaxies in the right panel of Figure 3 unsurprisingly have central peaks in the J/J_c distribution. The effects of resolution on the histograms themselves appears to be somewhat lower, and in fact we shall see that in fact the scatter in D/T values from the two simulations is closer to being constant in $\log D/T$. Interestingly, if we search for evidence of a small stellar disk to go along with the gas disk seen in the visual inspection of the first galaxy, we see that there is no evidence for one in the J/J_c distribution.

Although we do not plot J/J_c for the gas particles, we have examined their distribution and find it to be more rotationally supported than the stars, in agreement with previous work (see e.g., Mayer et al. 2008). The previous work on resimulated spiral galaxies has yielded D/T values from kinematic decomposition of e.g., 0.41 (Abadi et al. 2003b), 0.67-0.76 (Okamoto et al. 2007) 0.74 (Governato et al. 2004). Our example disk galaxies shown here are generally consistent with this range. From our large sample, we can say something about how rare truly disk dominated galaxies are in the simulation. At $z = 1$ only 3.5% of the galaxies in the *BHCosmo* run have D/T greater than 0.5. The maximum D/T value we find is 0.76 (a D/B ratio of 3.22). This is the same as the (mass weighted) D/T ratio of the disk galaxy simulated by Okamoto et al. (2007), which included AGN feedback.

Observationally, spiral galaxies in the local Universe are seen to have D/T ratios from unity (bulgeless disks) to ~ 0.1 (see for example Graham et al. 2001, who find a median D/T value of 0.75 for a sample of 86 face-on spirals). The D/T ratios are usually (and in the case of Graham et al.) calculated in terms of luminosity of each component, using fits to the photometry, rather than in stellar mass from the

kinematics, as we have done. This will tend to make our D/T rather lower because of the relative mass/light ratio of disks. Nevertheless, it is clear that the disk components of our galaxies are small, a fact related to the angular momentum problem in simulations. In separating galaxies into early and late types, we will therefore use a rather low value of D/T to divide the two classes (we use D/T=0.2.)

3.2 Projected stellar density profiles

There are a number of ways to decide on galaxy type using fits to the radially averaged luminosity profiles of galaxies. Galaxy classification based on photometry often makes use of the fact that early type galaxies are more centrally concentrated. For example, elliptical galaxies and the bulges of spirals tend to obey the deVaucouleurs profile well: $\Sigma \propto \exp(r/r_0)^{-1/4}$, and disk components have pure exponential profiles, $\Sigma \propto \exp(-r/r_{\text{eff}})$ (where Σ is the projected stellar density). A common method for using this information is to fit a Sersic profile which can account for both,

$$\Sigma = \exp(r/r_0)^{-1/n} \quad (1)$$

where n is the Sersic index (Sersic, 1968). At redshift $z = 0$ the largest study of Sersic index fitting was carried out by Blanton et al. (2005). At $z \sim 1$, there are quantitative measurements of the morphology from a variety of surveys including the CFHT legacy survey (Nuijten et al. 2005., using the Sersic index) COSMOS (e.g., Capak et al. 2007, using the Gini parameter).

To examine the stellar profiles of our simulated galaxies, we rotate them so that they are face on with respect to the stellar angular momentum vector. We then use this projected distribution to bin the stellar particles, assigning their masses to radial bins. Just as with the kinematics above, we are using stellar density rather than luminosity in a particular band.

In Figure 4 we show the projected stellar density profiles for our 20 example galaxies, again in the same order from top to bottom and with the late types on the left. We show results for the D4 run as a dashed line as well as the *BH-Cosmo* run in solid. The differences between the profiles for the two simulations appear to be much smaller than those in the kinematic decompositions in Figure 3. However, we shall see later that these small differences actually lead to large scatter in the best fit Sersic index for each galaxy in the two simulations.

In the left panels of Figure 4 we have also plotted an exponential disk profile, fitting it to the radial bins at greater distances than r_{half} from the center of the galaxy. We ignore the central bulge region within r_{half} in order to avoid biasing the fit, and also to avoid fitting the central profile inside the gravitational softening length of the simulation (1.4 proper $h^{-1}\text{kpc}$ for the *BH-Cosmo*). Looking at how well the late type galaxies obey a pure exponential profile, we can see that 4 out of the 10 have no significant bulge component, with the 6th from top being the best. A galaxy which is pure exponential all the way to the center was seen in the resimulation of Robertson et al. (2004). Here we see that this can happen relatively often, even with the comparatively low resolution of the D4 simulation.

In most of the panels in Figure 4 we can see that in the inner regions, the D4 simulation falls somewhat below the

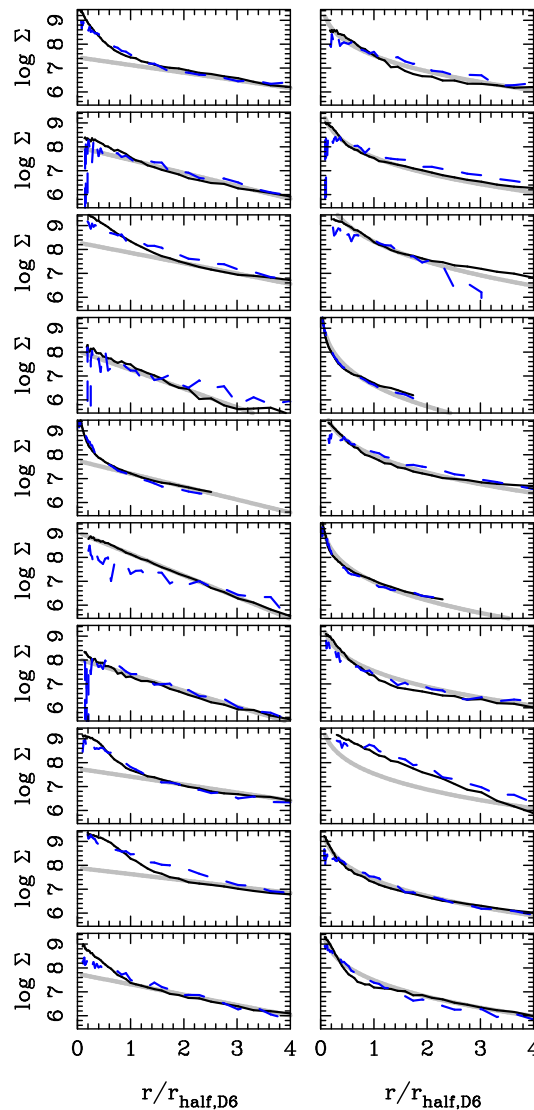


Figure 4. Projected stellar density profiles of the galaxies shown in Figure 1 (left column, late types) and Figure 2 (right column, early types). The thin solid lines are the profiles from the galaxies in the *BH-Cosmo* simulation and the dashed lines are the profiles for the same galaxies taken from the lower resolution D4 simulation. The units for Σ , the projected stellar density are $h^{-1}\text{M}_{\odot}$ (proper kpc) $^{-1}$. The x -axis is radial distance from the center of the galaxy, as a fraction of the half stellar mass radius (given for each galaxy in Figures 1 and 2). In the left panels we also show as thick grey lines exponential profile fits to the profiles (beyond the r_{half} radius) of the late type galaxies. In the right hand panels we show, also as thick grey lines de Vaucouleurs profile fits to the early-type galaxies.

higher resolution run. As found for example in the convergence tests of Governato et al. (2007), the inner parts of the galaxies are not resolved, so that we cannot say much about the structure of the bulges. Governato et al. (2007) estimate that several million resolution elements will be needed within the virial radius to do this.

Looking at the early types in the right panel, we can see that they are on average more centrally concentrated, as we noticed from looking at the images (Figure 2.) We have plotted a de Vaucouleurs profile fit to the profiles in these

images, and we can see that for 9 out of the 10 early types it gives reasonable results. We also see however that one of them (the 3rd from bottom) is also pretty close to exponential in shape, and the de Vaucouleurs profile is not a good fit at all. Returning to the image of this galaxy in Figure 2, it can perhaps be seen to be fairly smooth in the center, but there is no real hint that its profile is peculiar, nor is there in the kinematics Figure 3). This is quite surprising, and shows that even a good exponential profile is not necessarily a sign of a disk dominated galaxy.

In section 3.4, we shall instead fit a Sersic profile to all the galaxies, and use that to make a separation of galaxies into two classes. For now we have seen that for most of our 20 example galaxies there is reasonable agreement between the type suggested by their kinematics and their stellar profiles.

3.3 Resolution tests

We have mentioned two of the galaxy properties we are most interested in above, the D/T ratio and the Sersic index, n . We will also study the circular velocity, V_{circ} , the total angular momentum of different galaxy components (e.g., j_{gas}), the star formation rate, mean star formation redshift (z_{form}) and the exponential disk scale length, r_{disk} . For all these quantities, the numerical resolution of the simulation could influence the results. In this section we investigate whether changing the resolution causes a systematic bias by comparing the same galaxies in the *BHcosmo* and D4 runs. Because these simulations were run with the same initial random seeds to set up their initial conditions and have the same box size, in principle we should be able to find high and low resolution versions of the same galaxies. With such a resolution test, we will be able to get information on which of the parameters is most reliably computed by the simulation, in terms of both systematic bias with resolution and amount of scatter in results between the two resolutions. In order to emphasise the resolution difference between the two simulations, we refer to the *BHcosmo* run as the D6 run in this section (using the nomenclature of Springel & Hernquist 2003).

In order to carry out this test we first need to match up the galaxies in the D4 and D6 runs. We first apply a particle number cut which is equivalent to the 5000 particle lower limit for the D6 run. After applying this cut (439) particles we are left with 1297 D4 galaxies. For each D6 galaxy, we look for the closest (the smallest 3 dimensional separation between the centers, defined by the particle at the minimum potential) one in the D4 output. We also apply another criterion, so that the galaxies must be within 25 % of each other in total mass to be considered a match. We do not exclude galaxies which have already been matched. The procedure is insensitive to this, as is it is to changing the 25% matching criterion between 10% and 30%. In order to gauge roughly how many galaxies have been mismatched, we try applying the same mass similarity criterion to the dark matter masses of the galaxies. We find that none of the top 20 galaxies by mass change, but below that approximately 10% of the D6 galaxies are matched to another in the D4. We find similar results with the stellar mass, and so our conclusion is that approximately 10% of the galaxies are likely to be mismatched. This is a small number, but should

be borne in mind when considering the comparisons between simulations.

In Figure 5, we show the results for 9 different quantities, plotting the value for the D4 simulation against that in the D6 simulation, for each of the 1180 galaxies. In the plots we show two categories of galaxy, those which have > 439 particles in the D4 (equivalent to 5000 in the D6) as open symbols and those which have > 5000 particles in the D4 (equivalent to 57000 in the D6) as filled points. This is so that we can see whether any scatter or bias is less for larger particle numbers per galaxy. As the D6 galaxies all have > 5000 particles, in this sense the filled points will give a sense of the uncertainties induced by resolution on the results in the rest of the paper, which use the D6 outputs.

Looking at the different panels of Figure 5 we can see that all the galaxy parameters show correlations between the two simulations, although the scatter between them is in some cases (e.g., Sersic index, n) much larger than others, (e.g., V_{circ}). An $x = y$ line has been drawn on all panels and the first impression is that while the scatter may be large, there is not much evidence of strong systematic bias caused by decreased resolution. The most obviously different slope from 1 is that in the z_{form} panel. Here we can see that galaxies in the D4 simulation tend to form their stars on average significantly later than in the D6. For example, stars which formed at average $z = 3.5$ in the higher resolution model form at average $z = 2.5$ in the D4 run (for galaxies with between 439 and 5000 particles in the D4). The effect of the bias is seen to be significantly reduced when we move to galaxies with higher numbers of particles (the filled points). This bias with resolution is expected, given that at higher resolution smaller scale density fluctuations are present which can collapse earlier. A detailed study of star formation in the same multiphase model used in the present simulation was carried out by Springel & Hernquist (2003a) and to which we refer the reader for further resolution tests and interpretation.

Related to the star formation history is the current SFR at $z = 1$, which is also shown in Figure 5. In this case we can see that the SFR in the D4 run is systematically higher (the points tend to lie above the $x = y$ line) than for the D6 galaxies. This is particularly true for the low particle number galaxies. A possible interpretation is that perturbations which were not present in the D4 compared to D6 due to insufficient resolution are overtaken by collapse on larger scales and forming stars.

The two parameters which have the most scatter are the D/T ratio and the Sersic index n . The strength of the correlation between the two simulations can be judged using the Pearson correlation coefficient, which for D/T is 0.22 for all galaxies and 0.35 for D4 galaxies with > 5000 particles. The significance levels for the correlations are 10^{-14} and 2×10^{-5} respectively (there are ~ 10 times fewer galaxies for the high particle number subset, so the significance is lower). If we fit a straight line $y = a + bx$ to the D/T results we find an offset of $a = 0.21, 0.11$ for the small and large galaxies, respectively. This means that there is a small systematic offset, but it is in the direction of the low resolution galaxies having higher D/T ratios, not what one would expect if simple lack of resolution causes the angular momentum problem. This fit assumes that all the errors lie in the y -coordinate (the D4 D/T ratio) and gives slopes of $b = 0.54$ and $b = 0.60$.

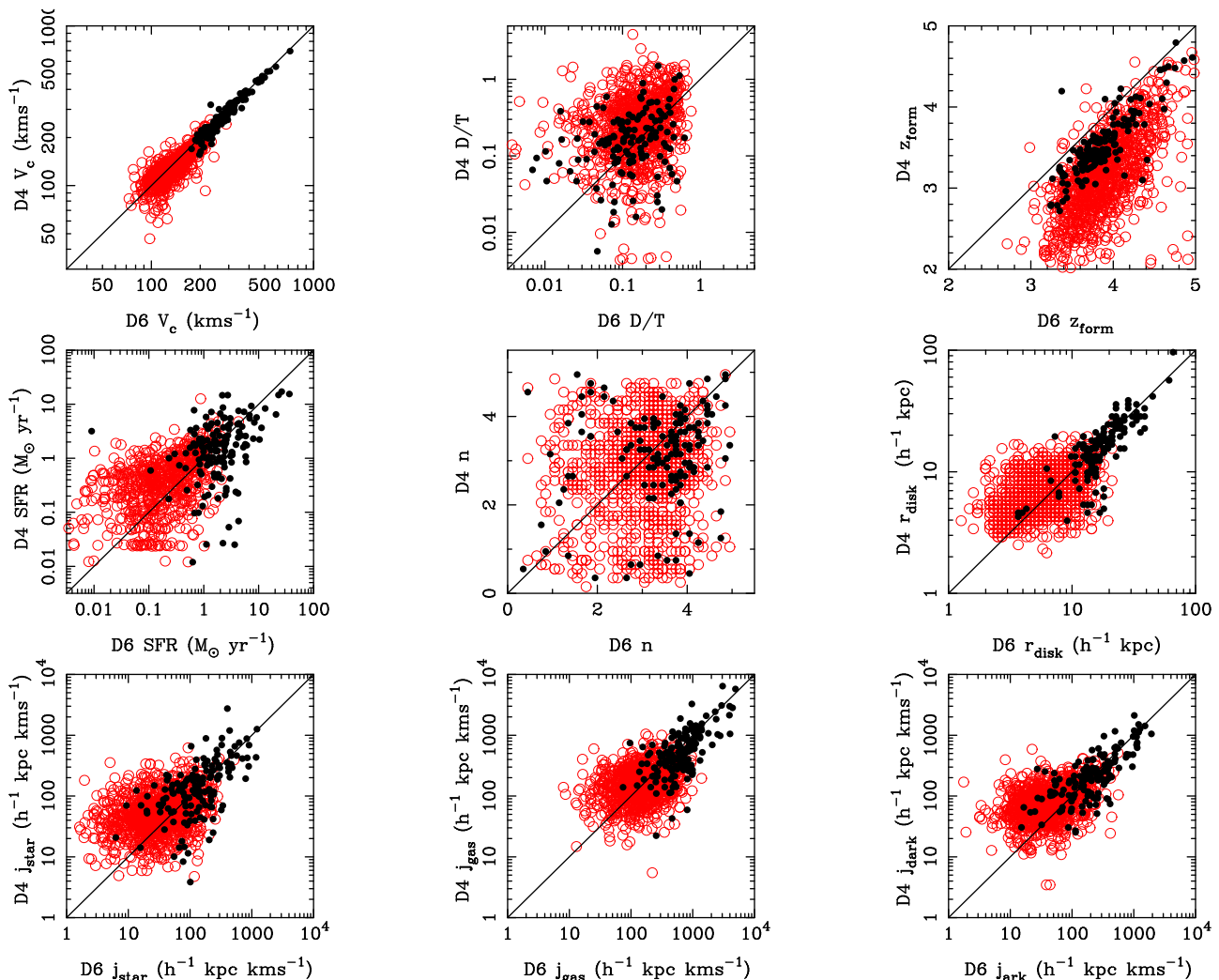


Figure 5. Comparison of galaxy properties in the *BHcosmo* (referred to here as the D6) simulation and the same galaxies selected from the lower resolution D4 run (see §3.3 for details of how the matching galaxies were found). In each panel, the open circles show galaxies which contain > 5000 particles in the D6 run, which corresponds to an equivalent of > 439 particles in the D4 run. The filled points are for galaxies which contain > 5000 particles in the D4 run (or the equivalent of 57000 for the D6). In the top row, we show from left to right the circular velocities of galaxies (measured at the 2.2 times exponential scale radius r_{disk} of the galaxies), the kinematically determined D/T ratio, the mean formation redshift of star particles in the galaxy. In the middle row we show the star formation rate, the Sersic index, and the exponential scale radius. In the bottom row are plotted the mean specific angular momenta of the stars, the gas and the dark matter.

The fact that the slope is not equal to one may be partly due to a significant portion of the scatter not coming just from the y -coordinate (i.e., the D6 value is inaccurate) and partly due to resolution lowering the angular momentum. Because the relevant “errors” in the x and y -coordinates are not known, it is not possible to say more than this.

For the Sersic index, we have a significantly worse correlation for all galaxies, $r = 0.11$, with a significance of 8×10^{-5} . For the > 5000 particle galaxies it is surprisingly good, $r = 0.84$ (significance $< 10^{-15}$). Visually, the scatter does appear to be very large, something that is interesting given the good correspondence between the lines showing the stellar profiles in the D4 and D6 cases in our plots of example galaxies (Figure 4). This shows that differences between the slopes of the profiles are quite subtle and that n may be a problematic indicator of galaxy type.

Given the evidence of the profiles seen in Figure 4, the physical gravitational softening length difference between the two simulations, ($1.4 h^{-1} \text{kpc}$ vs $3.1 h^{-1} \text{kpc}$) does not seem to make a difference to the Sersic indices.

The bottom three panels of Figure 5 show the resolution comparison of the specific angular momentum j of each of the three components, gas, dark matter and stars, of each galaxy. The scatter is relatively large, worse visually than the impression produced by V_{circ} and by r_{disk} . It does decrease with higher particle number and there does not appear to be a significant bias with resolution. This may mean that increasing resolution is not the whole story for dealing with the angular momentum (see e.g., Agertz et al. 2007) or else that with much higher resolution we might suddenly see a dramatic change (see e.g., Ceverino & Klypin 2007 for exploration along these lines). One fact which is obvious is

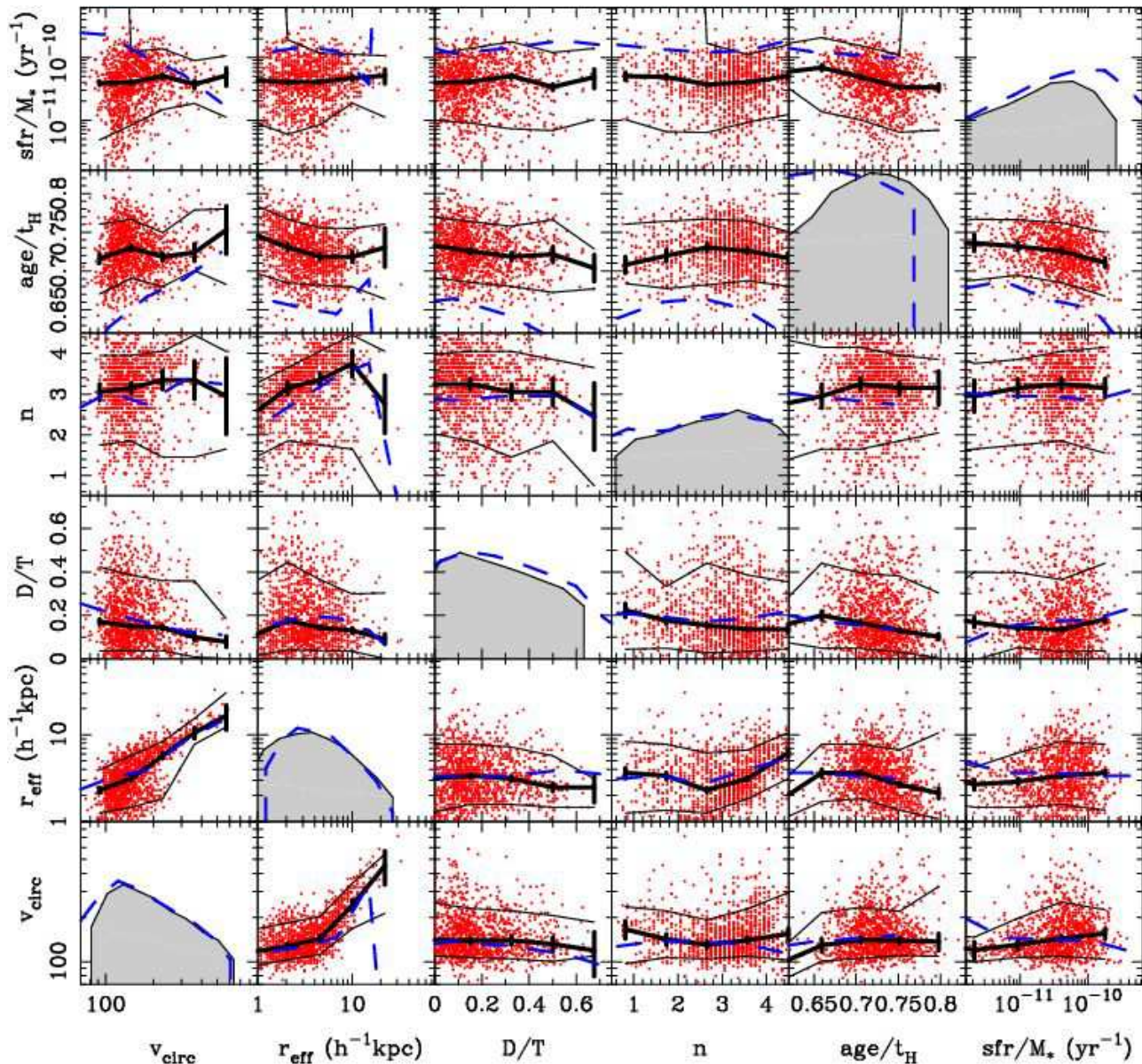


Figure 6. Galaxy properties in the *BHCosmo* simulation at redshift $z = 1$. In the panels which contain scatter plots, we show 1 point for each galaxy. We also show the median value in bins as a thick solid line, with Poisson error bars. The 90th and 10th percentile distributions in the same bins as the median are also shown as thin solid lines. The thick dashed line in each case shows results for the galaxies taken from the lower resolution D4 simulation. The diagonal panels show the probability distribution of the parameter values, on the same x -axis scale as the scatter plots. Again the dashed lines show the pdf from the D4 run and the solid line enclosing a shaded region the results from the *BHCosmo* simulation. The y -axis of the diagonal panels represents a logarithmic scale of probability. The overall normalization is arbitrary, but the height of each panel is 4 dex.

that the gas has higher j values than either the stars or the dark matter. We shall return to this in Section 3.5 below.

The conclusion we can draw from our study of identical galaxies at lower resolution is that most of the properties are robust, although the scatter between two resolutions can be large. It is largest for the Sersic index n and D/T ratios, two of the parameters we will use to separate our galaxies into different types. A relatively large systematic bias between parameters due to resolution effects is only present for mean stellar age, which is affected in the way one expects due to missing small scale power.

3.4 Correlations between galaxy properties

One of the aims of this paper is to see whether galaxy morphology in simulations is affected by environment. The other main aim is to see how galaxy properties are interrelated. For example, we look at whether disk dominated galaxies are smaller than bulge dominated ones, how Sersic index is related to D/T ratio and so on. Our main tool in this regard is a scatter plot of 6 important galaxy properties where each is plotted against the 5 others. This is shown, for $z = 1$, the redshift we are focussing on (for the *BHCosmo* run) in Fig-

ure 6. For each of the quantities we show a histogram of the values on the diagonal (where the y -axis is in log units).

We have seen in Figure 4 that it is possible to roughly fit an exponential profile to the region outside the inner half stellar mass radius, even when the galaxy is an early type. In this way, we have computed an effective radius r_{eff} for all galaxies, so that we can compare early and late types on the same footing. We use this value in our measurement of the galaxy circular velocity, which we compute using

$$V_{\text{circ}} = \sqrt{GM_{<2.2r_{\text{eff}}}/r_{\text{eff}}}. \quad (2)$$

Here $M_{<2.2r_{\text{eff}}}$ is the total mass within 2.2 effective radii (e.g., Courteau 1997). Our V_{circ} values for all galaxies are therefore computed in this way. We use r_{eff} in order to be consistent with observational definitions of circular velocity, but find no significant difference to our results if we instead use r_{half} .

In the panels of Figure 6, we show lines which represent the medians of the points in bins, as well as the 10th and 90th percentile lines. For the median, as well as the pdfs, we show results for the D4 run as a dashed line. We note that half of the panels are repeated, in a different orientation. We include them because seeing the median of the other quantity is still useful.

A number of interesting facts are apparent from a look at Figure 6. The narrowest relation is between r_{eff} and V_{circ} . Galaxies with $V_{\text{circ}} = 200 \text{ km s}^{-1}$ have a median r_{eff} of 4 proper $h^{-1}\text{kpc}$, or 5.7 kpc. This can be compared to the Milky way, which has $r_{\text{eff}} = 3.5 \text{ kpc}$, for example. It seems that the size of galaxies in the simulation is therefore roughly correct, at least within a factor of 2. The main problem, as we shall see from the D/T ratios is that they have bulges which are too large. The values of r_{eff} and V_{circ} can be seen from Figure 6 to be unaffected by resolution.

Moving on to the D/T ratios, we can see that there is a trend for disk dominated galaxies to be smaller (lower V_{circ} and r_{eff} values) than systems with greater bulge components. The median D/T value for the smallest galaxies plotted ($V_{\text{circ}} \sim 100 \text{ km s}^{-1}$) is approximately twice that of the largest ($V_{\text{circ}} \sim 500 \text{ km s}^{-1}$). This trend can also be seen in the 90% envelope, and the 10% envelope, which both trend downwards with galaxy size. There is a particularly obvious lack of disk galaxies above $V_{\text{circ}} \sim 300 \text{ km s}^{-1}$. Even at $z = 1$, therefore the simulations exhibit the well known observational trend for the largest galaxies to be early types. While the trend of D/T with size does seem to be reasonable compared to observations, the absolute values are low, as we have seen before. For example, there is a lack of disk galaxies which have no detectable bulge, but which are known to exist in the local Universe (e.g., Dalcanton & Bernstein 2000).

If we look at the age of galaxies next, it becomes apparent that the behaviour of galaxy property trends in the presence of large scatter is quite complex. For example in the panel of V_{circ} vs age, the higher V_{circ} galaxies are slightly older in the median, although the errors are large. On the other hand, in r_{eff} vs age, the smaller galaxies (these with $r_{\text{eff}} < 5h^{-1}\text{kpc}$) have higher ages. Conversely, the lower D/T galaxies also have higher ages, as we would expect of late types. We find therefore that some of the usually assumed relationships between galaxy properties and type (see e.g., Maller et al. 2006, Koda et al. 2007) hold, but in the grid

there are several counterexamples. The effect of resolution on galaxy ages is for them to be lower in the D4 run, as we have seen in Section 3.3. This effect is shown by the median line in the panels of Figure 6. We do see however that although the ages are lowered by a constant offset, the trend of the ages with other properties is broadly similar to the higher resolution run in all the panels.

The Sersic index, n , of the galaxies can be seen to increase with r_{eff} (although the last r_{eff} bins drops down, the errors are large). Diskier galaxies also have slightly lower n values, as we would expect, with the median n for galaxies with D/T > 0.5 being around 2.8 ± 0.2 compared to 3.2 ± 0.05 for galaxies which are purely ellipticals (D/T = 0 < 0.1) The older galaxies also have slightly higher n values, and the dependence on n on V_{circ} is basically flat.

We note that Hopkins et al. (2008) have recently shown that fitting a single component Sersic profile can mischaracterize the profile shape of post starburst ellipticals. As we have seen with the profiles plotted in Section 3.2, kinematically selected early types can have low Sersic indices. Hopkins et al. used two component Sersic fits to examine the inner and outer profiles of simulated merger remnants. A median Sersic index for the outer profile found by Hopkins et al. is $n \sim 2 - 3$ (e.g. see their Figure 15). Although our mass and spatial resolution is not high enough to permit two component fits here, this issue should be borne in mind when using n to separate galaxies into morphological classes (e.g., see Section 4.3)

The specific star formation rate, in the top row of Figure 6 is pretty flat in the median with respect to the other properties. The strongest apparent trend is with galaxy age where it can be seen that both the median sSFR and the 10%-90% envelope do drop with increasing age. The envelopes do tend to widen also at low r_{eff} and V_{circ} , indicating that galaxies are more extreme with respect to sSFR when they are small.

Looking at Figure 6 overall, we can see that there are many instances of the expected trends between properties which we know from observations (e.g., Blanton et al. 2003). For example galaxies are usually classified into ‘‘early’’ and ‘‘late’’ types where one can broadly say that early types are larger, have older stellar populations and larger bulges than late types. Of the 15 panels in Figure 6 which carry independent information, 10 of them fit into this simple picture (for example, galaxies seen kinematically to have larger disks do have smaller Sersic indices), 1 runs counter to it (we find that older galaxies are smaller, as measured by r_{eff}) and 4 are neutral (sSFR exhibits little median variation with other properties). It is beyond the scope of this paper to examine any of these relationships in detail, but it is apparent that simulations are nearing the point where in future work it will be profitable to do so and make more direct comparisons with observational data.

3.5 Angular momentum

Simulations of disk galaxy formation have historically had problems with excessive angular momentum loss, leading to stellar components with bulges too large compared to observations (Mayer et al. 2008 for a review). These include for example the zoomed simulations of Sommer-Larsen et al. (2003), Abadi et al. (2003ab), Robertson et al. (2004).

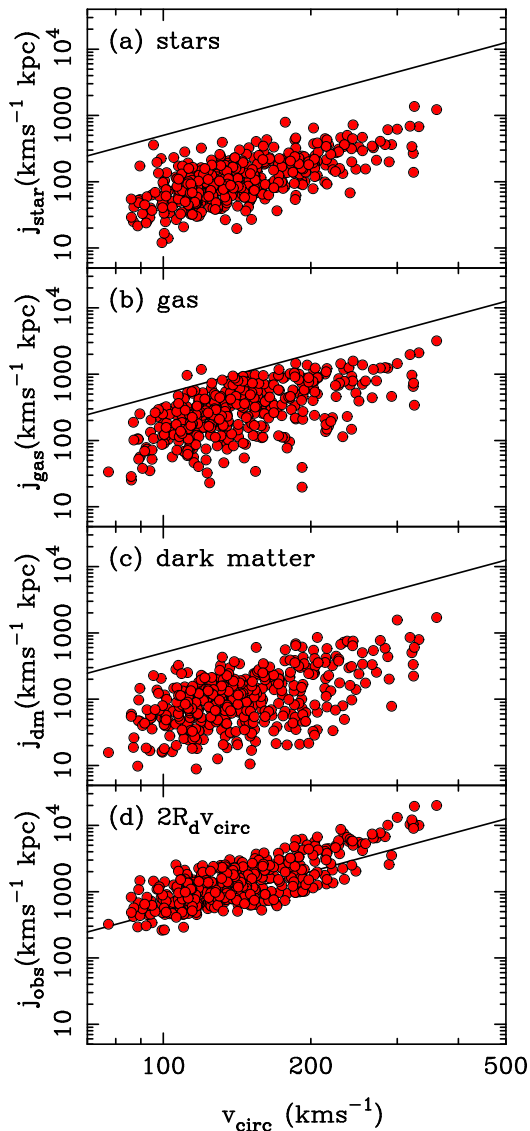


Figure 7. Rotation speed vs specific angular momentum j at redshift $z = 1$ for late type galaxies in the *BHCosmo* simulation (points). Only galaxies with a D/T ratio > 0.2 are shown, the same threshold used to define late types in the rest of the paper. From top to bottom are results for the stellar component, the gas and the dark matter. The bottom plot shows an estimate of the specific angular momentum that is not computed directly from the angular momentum of the particles but instead by multiplying the disk scale radius by twice the circular velocity. This is the estimator used for observational data (e.g., Courteau 1997) and is valid for an exponential disk. The solid line in each panel is taken from Abadi et al. (2003a), and describes well the median relation seen in the observational ($z = 0$) data compilation of Navarro (1998). In order to compare directly to Abadi et al. (2003a) we have rescaled using $h = 0.65$ when computing the values of j .

Robertson et al. (2004) and Abadi et al. (2003ab) pointed out that exponential galactic disks could be formed which were of the correct size, but which were deficient in specific angular momentum. Governato et al. (2007) and Ceverino & Klypin (2007) have most recently been able to form disks which were closer to being realistic, through a combination of high resolution and modelling of star formation and feed-

back. All of these simulations were zoomed runs, however, and it is not clear to what extent these results are dependent on the histories of the individual halos selected for resimulation.

A clear way to describe the extent of any potential angular momentum problem is to plot the specific angular momentum content of galaxies as a function of their circular velocities. This has been done by for example Navarro & Steinmetz (2000) and Abadi et al. (2003a), comparing the simulation results against the observational compilation of Navarro (1998). Observations of the specific stellar angular momentum content of disk galaxies were made using an estimator which combines the observed circular velocity and disk scale length (Courteau 1997), so that $j_{obs} = 2R_{eff}V_{circ}$. For the simulations, the circular velocity is usually computed using Equation 2, but the angular momentum is summed directly from the star particles.

In Figure 7 we show results from the *BHCosmo* simulation at $z = 1$. It is important to note that the simulated galaxies we are plotting are from $z = 1$ whereas the observations (Mathewson et al. 1992, Courteau 1997) were made at $z \sim 0$. Based on the lack of evolution in angular momentum vs V_{circ} seen in the D4 run (which was run to $z = 0$) we expect this to make little difference to the comparison. The straight line in Figure 7 is taken from Abadi et al. (2003a). It describes the mean of the observational data well. For the simulation points, because we are comparing to observational data for disk galaxies, we apply a threshold on the D/T ratio before plotting points in Figure 7. This threshold is at a D/T ratio of 0.2, which selects 40% of the galaxies to be disks at this redshift, $z = 1$. Although this cut is essentially arbitrary (we have a smooth continuum of D/T ratios for galaxies), we will see later (Section 4.3) that it enables us to reproduce very approximately the fraction of morphologically classified galaxies of early and late types as a function of density. For the points in Figure 7 we measure j , the specific angular momentum by summing the total angular momentum of the particles in question (we deal with stars, gas and dark matter separately in the different panels) and dividing by their summed mass. We use only particles within 2.2 times R_{eff} , in order to be consistent with observations, and include all particles interior to that radius, including those in the bulge.

We can see in the top panel of Figure 7 that the median j_{star} is a factor of ~ 8 lower than the observational value for disk galaxies. As we have seen in the distribution of D/T ratios, simulated galactic stars have too little orbital angular momentum. This result is somewhat better than the lower resolution runs of Navarro & Steinmetz (2000), who were a factor of ~ 30 below the observations, but the angular momentum deficit is still large. Robertson et al. (2004), with somewhat better resolution in their resimulated galaxies (a dark matter particle mass of $3 \times 10^6 h^{-1} M_{\odot}$, 4 times smaller than Abadi et al. 2003a) formed a spiral with j_{star} approximately a factor of 2 below the observational trend. This galaxy, with a quiet late merger history is similar in its j_{star} to many of our galaxies. Our results are therefore likely to be similar to theirs, except that we have access to a whole population of simulated galaxies.

The median gas specific angular momentum in Figure 7 is closer to the observational line than the stars. This was also seen by e.g., Abadi et al. (2003a) and Robertson et al.

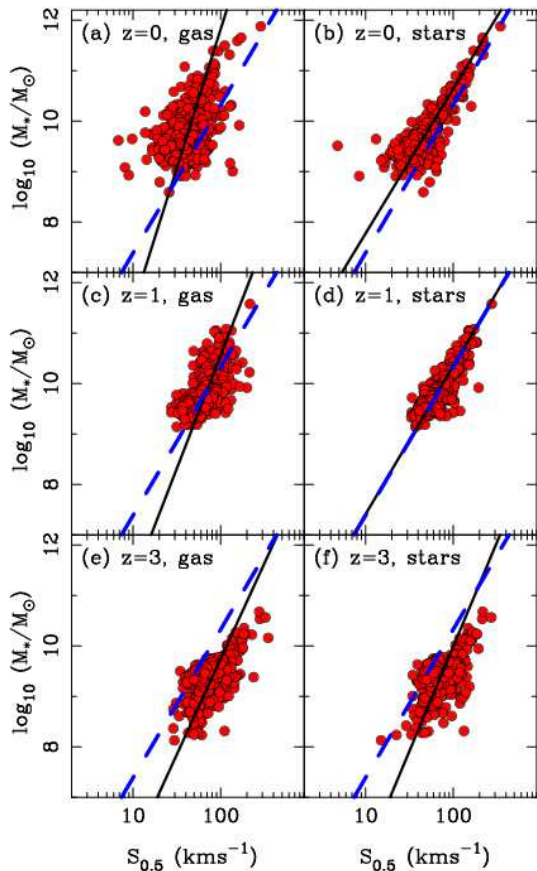


Figure 8. The stellar mass Tully-Fisher relation for late type galaxies (selected using $D/T > 0.2$) in the *BHCosmo* simulation (at redshift $z = 1$ and $z = 3$) and the *D4* simulation ($z = 0$). The x -axis is the statistic $S_{0.5}$ from Kassin et al. (2007), which is a kinematic estimator of support from disordered and ordered motion (see equation 3). $S_{0.5}$ from the simulations was computed either using gas particle velocities (left panels) or star particle velocities (right panels). The solid line shows a best fit power law relation to the simulation data in each panel. The dashed line is the best fit power relation from Kassin et al. (2007) to their observational data. This observational fit is the average relation measured from 4 bins varying in redshift from $z = 0.1 - 1.2$. Kassin et al. (2007) find no statistically significant variation with redshift.

(2004), who find that as gas cools and stars form, angular momentum is lost to the galactic halo. For the dark matter, the j_{dm} values are closer to those seen in the stars, (as also seen by Abadi et al. 2003a), although the scatter in j_{dm} for a given V_{circ} is larger.

Although the angular momentum content of the disks is low, we find that the size of the disks is actually reasonable compared to observations. To show this, we plot in the bottom panel of Figure 7 the observational estimator for the specific angular momentum of stars, j_{obs} . In this case, we find that the median is compatible with the observational line. Therefore, as seen by Robertson et al. (2005) in a single galaxy, the disks are of reasonable scale, but they have a bulge component which is too large, so that too much of the galaxy is supported by non-circular motions.

By looking at the angular momentum content of ~ 500 disk galaxies, we see that the problem seen in resimulations

of a small number of galaxies persists. The addition of black hole accretion and feedback to our runs compared to those mentioned above does not noticeably impact the excess population of non-rotationally supported stars. This is compatible with the recent work of Okamoto et al. (2007) who resimulate disk galaxies with and without black hole feedback.

3.6 Stellar mass Tully-Fisher relation

The Tully-Fisher (1977) relation (hereafter TFR) between the luminosities of galaxies and their rotation velocities has long been used as a test of galaxy formation models (e.g., Steinmetz & Navarro 1999). For example, the amplitude and zero point of the TFR seen in observations at $z \sim 0$ is still difficult to reproduce in high resolution simulations of disk galaxies (Portinari & Sommer-Larsen 2007). The stellar mass-rotation velocity version of the TFR is easier to compute theoretically. It has recently been measured out to $z = 1.2$ using observational data from the AEGIS and DEEP2 surveys (Kassin et al. 2007). In the usual $M-V_{\text{rot}}$ version of the TFR, where M is the galaxy stellar mass and V_{rot} there is a strong dependence of scatter in the relation on galaxy morphology (disturbed, close pairs etc.). Kassin et al. (2007) however find a modification of the TFR which works well with minimal morphological pruning and holds over the entire redshift range $z = 0.1 - 1.2$.

The relation computed by Kassin et al. is between M and $S_{0.5}$, where the latter is a kinematic estimator which combines dynamical support from ordered motion with that from disordered motion (see Weiner et al. 2006). The quantity $S_{0.5}$ is computed using

$$S_{0.5}^2 = 0.5V_{\text{rot}}^2 + \sigma_g^2, \quad (3)$$

where V_{rot} is the rotation velocity of galaxy on the flat part of the rotation curve, σ_g is a gas velocity dispersion, both being measured from a two-dimensional fit to emission line in the galaxy spectra. Kassin et al. find the observed $M-S_{0.5}$ relation to be fairly tight, with an rms intrinsic scatter in $S_{0.5}$ of 0.10 dex. The slope and amplitude of a log-log fit to the points, $\log_{10} S_{0.5} = a + b \log_{10} M / 10^{10} h^{-1} M_{\odot}$ is $a = 0.34 \pm 0.05$ and $b = 1.89 \pm 0.03$ averaged over 4 bins in redshift ranging from $z = 0.1 - 1.2$. The fits are not significantly different for all redshift bins.

We compute M and $S_{0.5}$ values for disk galaxies in our simulations. Disk galaxies are again taken to be those for which $D/T > 0.2$. The M values are straightforward: we use the total mass in star particles in each galaxy's subhalo. For $S_{0.5}$ we have a choice, whether to use a quantity measured from particle velocities in the simulation, or whether to use the mass within a certain radius to compute a value of V_{rot} , assuming rotational support. In order to include the effect of non-rotational motions, we do the former. For V_{rot} , we compute the mean rotational velocity of particles in a radial bin of width r_{eff} centered on a radius $2.2r_{\text{eff}}$ from the center of each galaxy, and we compute σ_g from the scatter of particle velocities about V_{rot} . Using these quantities, we estimate $S_{0.5}$ for the simulated galaxies. For each galaxy, we compute two versions of $S_{0.5}$, one using gas particle information, which more closely corresponds to the observational information, and another using the star particles.

The results are shown in Figure 8, where we show $S_{0.5}$ computed from both gas and stars for 3 different redshifts.

For $z = 1$ and $z = 3$, we use the *BHCosmo* simulation, whereas at $z = 0$ we use the D4 run. We also show the power law relation which is the average one for the data of Kassin et al. (2007) over $z = 0.1 - 1.2$. For each panel, we also compute the best fit power law relation from our simulated data and show it as a solid line. In computing the fit, we follow Kassin et al. and assign the intrinsic scatter (in this case we assume all the scatter is intrinsic) to the $S_{0.5}$ coordinate.

We notice from Figure 8 that the $S_{0.5}$ values computed from the gas have a larger scatter about the mean relation than the stars. The rms scatter in $S_{0.5}$ ranges from a maximum of 0.16 dex for the gas at $z = 0$ to a minimum of 0.08 for the stars at $z = 1$. This is not too dissimilar from the observational data, which has $S_{0.5}$ intrinsic scatter ranging from 0.08 to 0.12 dex over 4 redshift bins. As with the observations, we find no systematic change in rms scatter with redshift. It can also be seen that fits to the stellar simulated $S_{0.5}$ values are consistent with the observed fit. The largest discrepancy is at $z = 3$, a higher redshift than yet reached with the observational data, for which the slope is $b = 0.24 \pm 0.02$, less than 2σ different. The $S_{0.5}$ values computed from the gas particles do appear to have a systematically slightly steeper slope than the observations (we find $b = 0.22 \pm 0.03$ averaged over all 3 redshifts), but this is less significant than the $\sim 4\sigma$ discrepancy in the intercept, a which is seen at $z = 0$.

Overall, we therefore find that the stellar mass TFR relation (between M and $S_{0.5}$) measured in the simulations does not change in slope with redshift (between $z = 0$ and $z = 3$) and is consistent with the slope seen in the observational data of Kassin et al. (2007). The zero point measured from the gas properties in the simulation is somewhat noisy, but not systematically different when averaged over all redshifts.

3.7 Orientation

The relationship between a galaxy’s morphology and angular momentum can give important clues to the processes that occurred during its formation. A way to measure this quantitatively is to measure the alignment between the first-ranked principal axis of inertia of a galaxy and its angular momentum axis. We have carried this out for all galaxies in the *BHCosmo* simulation, again at $z = 1$, including the low D/T ratio galaxies.

We compute the inertia tensor for each galaxy and diagonalize it, to find the principal axis with the largest moment of inertia. We do this separately for each component of the galaxy, using every particle in the subgroup. From the scalar product of this axis with the angular momentum axis, we find an alignment angle, θ . The pdf of θ values is shown in Figure 9. We find that the gas component of galaxies is most strongly aligned, with a pronounced peak close to zero degrees, likely to be coming from the gas disks seen in many galaxies (for example, even the early type galaxy in the top panel of Figure 2 had a pronounced gas disk. The median value for the gas is $\theta = 25.7^\circ$, significantly more aligned than the stars ($\theta = 39.0^\circ$). The stellar alignment angles do have a low θ peak, however, indicating that rotationally supported stellar disks are still common. By looking at the orientations of galaxy shapes in Figure 2 (where the

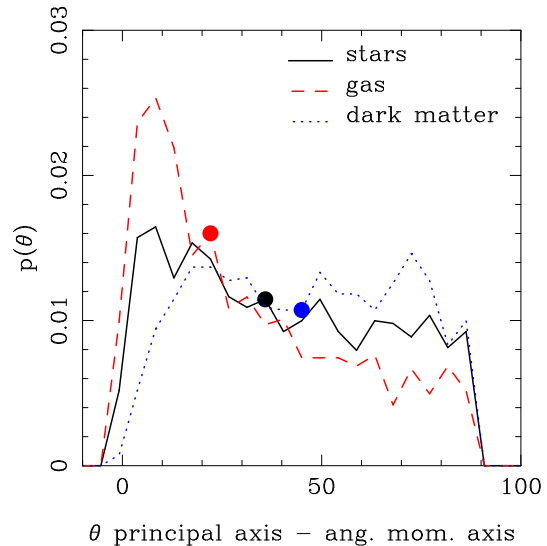


Figure 9. Histogram of the angle (in degrees) between the principal axis measured from the inertia tensor and the angular momentum axis, for galaxies in the *BHCosmo* simulation at redshift $z = 1$. We show results for the stars, gas and dark matter distributions, but the angle in each case is measured from the angular momentum axis computed from the stars. The solid points show the median angles (25.7° for gas, 39.0° for stars, and 48.3° for dark matter).

projections are defined by the A.M. axis) we can see that the misaligned galaxies are indeed likely to be mostly early types, as we would expect. Finally, in Figure 9 we can see that the dark matter halos are also noticeably flattened perpendicular to the rotation axis (the same flattening direction as the gas and stars), with a median alignment angle of $\theta = 48.3^\circ$. The expectation value for the median of a random distribution is $\theta = 60.4^\circ$, with a Poisson error of 1.8° . As the dark matter is dissipationless, this flattening could be partly due to adiabatic contraction in response to the rotationally flattened gas and stellar component. A strong effect was also seen by Bailin & Steinmetz (2005) in purely dissipationless simulations.

Looking at the alignments of the angular momentum vectors of the different components themselves can also give us some clues to how the rotational support arises. In figure 10 we plot the distribution of alignment angles ϕ of the star and gas angular momentum axes with the dark matter angular momentum axis for each galaxy. We find that there is a strong alignment of the stellar A.M. with the dark matter A.M. (median angle $\phi = 43.5^\circ$), and a somewhat weaker alignment of the gas with the dark matter (median $\phi = 69.6^\circ$). This is quite surprising given the alignment of the principal axes of the gas seen in Figure 9. We have also computed (not plotted) the alignment of gas and star angular momentum vectors. We find a median angle in this case of $\phi = 61.6^\circ$, closer to the alignment of the gas and dark matter. We can therefore see that the stellar angular momenta appear to have become correlated with that of the dark matter *after* the stars have formed from the gas. This coupling through collisionless dynamics could perhaps be a numerical effect, due to two body interactions. To provide additional information, we have investigated our lower resolution simulation, the D4 and found that the rank order

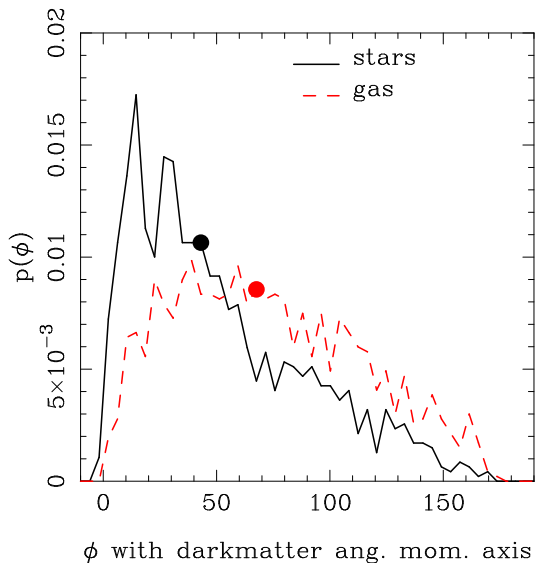


Figure 10. The alignment angle, ϕ (in degrees) between the star and gas angular momentum axes and the dark matter angular momentum axis, for galaxies in the *BHCosmo* simulation at redshift $z = 1$. The solid points are the medians of the distributions (43.5° for stars and 69.6° for gas).

of the median alignment angles are the same as for the *BH-Cosmo* run, i.e. star-dark, star-gas, gas-dark, in order of best to worst alignment. The median angles of the latter two are $\sim 10^\circ$ worse, but for star-dark, the angle is $\sim 20^\circ$ worse, suggesting that the stellar angular momentum is affected by the most by lack of resolution.

We note that in the simulations of Van den Bosch et al. (2002), a much stronger alignment was seen between the angular momentum of the (adiabatic) gas in halos and the dark matter (median angle $\phi = 27.1^\circ$) than here, so that without dissipation, the gas is much more strongly coupled in its rotation to the dark matter.

3.8 Age of disk and bulge stars

We have seen in Figure 6 that galaxy ages do have some dependence on other properties, including size and D/T ratio. We have decomposed the galaxies kinematically into bulges and disks (Section 3.1), and so it is of interest to see whether the ages of the disk and bulge stars fit into this general picture. In Figure 11, we have plotted the mean redshift of formation of stars in the disks and bulge components of the galaxies in the *BHCosmo* run at $z = 1$. We show the galaxies with D/T ratios greater than 0.2 (our fiducial threshold between kinematically defined early and late types) as red points.

We can see that the cloud of points extends down to low redshifts, indicating that the disk component of galaxies does indeed form significantly later than the bulge. For example, there are essentially no bulges with a mean star formation redshift below $z = 3$, but disks continue to form all the way down to $z = 1$, the lowest redshift possible. The disks below $z \sim 2$ are all disk components of bulge dominated galaxies, so that they only represent a small fraction of the galaxy. Interestingly, we also see that the disks with

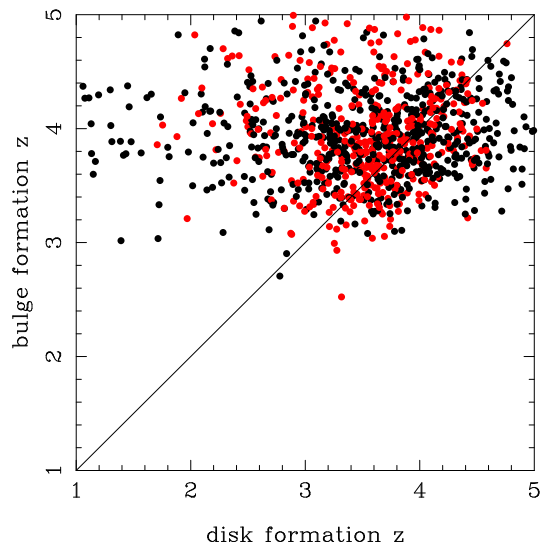


Figure 11. The mean age of star particles defined kinematically to be in a disk component, versus the age of those in the bulge, for galaxies in the *BHCosmo* simulation at redshift $z = 1$. We show results for late type galaxies (D/T > 0.2) as red points and early types as black points.

the highest formation ages $z \gtrsim 4.5$ also belong to early-type galaxies.

4 RELATION BETWEEN ENVIRONMENT AND GALAXY PROPERTIES

In the previous section we have seen that individual galaxy properties in the simulations are by and large what we would expect given a mixture of early and late types. We will now investigate how the immediate environment has affected these properties.

4.1 Measures of environment

We use four different definitions of the local environment of a galaxy, in order to span a range of parameters from those close to what can be measured observationally to measures related directly to the dark matter distribution. The first measure is the density computed from the distance to the tenth nearest galaxy. For this we use positions for galaxies above our 5000 particle threshold, and compute a local density for each galaxy, dividing the density of the sphere enclosing 10 neighbours by the mean density of galaxies in the simulation. We label this quantity on the plots as $\rho / \langle \rho \rangle$. The density computed from the tenth nearest galaxy is often used in observational measurements, such as in the morphology-density relation of Dressler (1980), and subsequently by Dressler et al. (1997), Smith et al. (2005), Carpak et al. (2007) and others. In these cases, the measurement is made in 2 dimensions, from the projected positions of galaxies, but the two quantities will be closely related. We explore this measure more closely in the next section.

A related measure is ρ_{13} , which is the density computed from a sphere centered on the galaxy which contains $10^{13} h^{-1} M_\odot$ of dark matter. In practice, this will be very similar to the first measure, based on galaxies, but will be

less noisy. It will also be more directly related to the gravitational influence of nearby structures, being based on mass density and not number density. We note that a very similar measure of environment, computed from the radius of a sphere which contains $10^{13}h^{-1}M_{\odot}$ of all types of matter was used by Colberg & Di Matteo (2008) in their study of the environmental dependence of black hole properties in the same simulation (the *BHCosmo* run) which we use here.

The galaxies are members of friends-of-friends groups of particles, and so we can also categorise their environment using these groups. We use the mass of the FOF group as one means of quantifying their environment, and the other the distance of the galaxy from the FOF group center of mass, in units of the virial radius, r_{200} . We compute r_{200} by measuring the radius of a sphere which contains 200 times the mean density.

4.2 Galaxy properties and environment at $z=1$

In Figure 12, we use the same galaxy parameters which were shown in Figure 6, but this time instead of plotting them against each other, we plot them against our four measures of local environment. We again show the situation at $z = 1$, for the *BHCosmo* simulation. Before proceeding with our analysis we note that at $z = 1$ there are no rich clusters in the relatively small simulation volume. (the largest FOF group has a mass of $6 \times 10^{13}h^{-1}M_{\odot}$). Below we will see that this will affect our ability to compare to observational data for the high density end of environments at this redshift. In interpreting Figure 12 we should therefore bear in mind that the dense environments in the plot are groups rather than clusters. In order to look at galaxies in clusters at high resolution, a resimulation approach should be used (see for example Saro et al. 2006.)

Looking at the figure, we can immediately see that the results are a mixture of relationships which we would have expected and some which are surprising. The values of V_{circ} for galaxies increase steadily with density, both $\rho/\langle\rho\rangle$ and ρ_{13} , the median rising by approximately a factor of 2 over 3 orders of magnitude in density. For V_{circ} vs M_{grp} , we see that there is an upper envelope of large galaxies in each group, but also that when M_{grp} reaches $2 \times 10^{12}h^{-1}M_{\odot}$, there are enough satellite galaxies to pull the median V_{circ} value down. In terms of r/r_{200} , we can see that the galaxies with the very highest V_{circ} values are indeed close to the center of mass of the FOF groups. There is a large cloud of points, between 0.1 and ~ 1.0 virial radii from the center, indicating where most of the galaxies are found. The number density of points decreases rapidly beyond r/r_{200} , although a few galaxies are found at distances of up to 10 virial radii. The median of V_{circ} values does not vary with r/r_{200} .

The variation of r_{eff} with density is similar to V_{circ} , except that the effect of satellite galaxies appears to be more pronounced. Also, even the median r_{eff} value changes with r/r_{200} .

Moving on to the D/T ratio in the third row from bottom of Figure 12, we find more complex dependencies on density. There is a moderate rise in the median D/T ratio, from 0.13 to 0.2 as $\rho/\langle\rho\rangle >$ changes by 3 orders of magnitude. It therefore seems as though there are many small bulge-heavy galaxies at low densities. This behaviour is also repeated but more weakly (only significant at the $\sim 1\sigma$ level)

when looking at ρ_{13} . If we look at the relationship between D/T and r/r_{200} we can see that the median D/T rises towards the edges of groups, significant at the $3 - 4\sigma$ level, and the 90th percentile line increases dramatically. There are therefore not many disk dominated galaxies in the centers of groups. This seems to be opposite to the trend seen in the variation of D/T with density. However, it is possible that the D/T values do go down with very high densities, but that this is not easy to see with the relatively noisy density estimators that we have (the 90th percentile of D/T does appear to decrease for large ρ_{13} .) When comparing r/r_{200} and ρ values we should bear in mind that when large galaxies are present, the group center of mass better correlates with the centers of large galaxies, and hence the density. This can help explain some of the apparent differences in behaviours with r/r_{200} and ρ .

The variation of Sersic index, n with density is basically consistent with flat from low to moderate density, followed by a decline in the median value, indicating fewer centrally concentrated early types at high density. This is somewhat consistent with the trend seen in D/T ratios, although in that case more variations were seen at low density than high. For n , the errors are large, but it does seem from the 90th and 10th percentiles that late types preferentially prefer the outskirts of groups as well.

The mean stellar age of galaxies does not appear to vary much with density at this redshift. There is perhaps even a small hint that galaxies in low density regions are slightly older, something which is puzzling but consistent with the slight preponderance of bulge-dominated systems there.

The specific star formation rate of galaxies in our simulations rises slightly with density, but also on the outskirts of groups. While the trend seen in observations at $z = 1$ by Cooper et al. (2008) has the same sign as that seen at low redshifts (e.g., Gomez et al. 2003), Cooper et al. find that the total SFR has an inverted relation with density. The behaviour and comparison with observations, particularly of the total SFR is investigated fully in this *BHCosmo* simulation by Colberg & Di Matteo (2008). For now, we note that the specific SFR trend we plot is roughly consistent with what has been seen with the D/T ratio and Sersic index, i.e., a reversal, or at least flattening of the trends seen in galaxy morphology with environment at redshift $z = 0$.

Some of the trends of galaxy properties with density do have some dependence on galaxy mass/particle number. For example when we limit ourselves to plotting galaxies containing 25000 particles instead of 5000 (although we still use all galaxies to compute $\rho/\langle\rho\rangle$), we find that the median D/T value for the highest $\rho/\langle\rho\rangle$ bin drops by 2σ to D/T=0.1. The previous bins are essentially unchanged. It is therefore possible that the efficiency of destruction of spirals in the highest density regions depends on particle number. In this test, the qualitative behaviour of SFR is unchanged, but the highest density bin does have slightly older galaxies.

Our overall conclusion from Figure 12 is that at $z = 1$ the relationships between galaxy properties and density in our simulations are complex. The preponderance of late types in low density regions seen at $z = 0$ seems to be reversed, with higher star formation rates in high densities. At the very highest densities, there are hints that the disk fraction may decrease, but this is dependent on resolution/particle number, with the main uncertainty that our

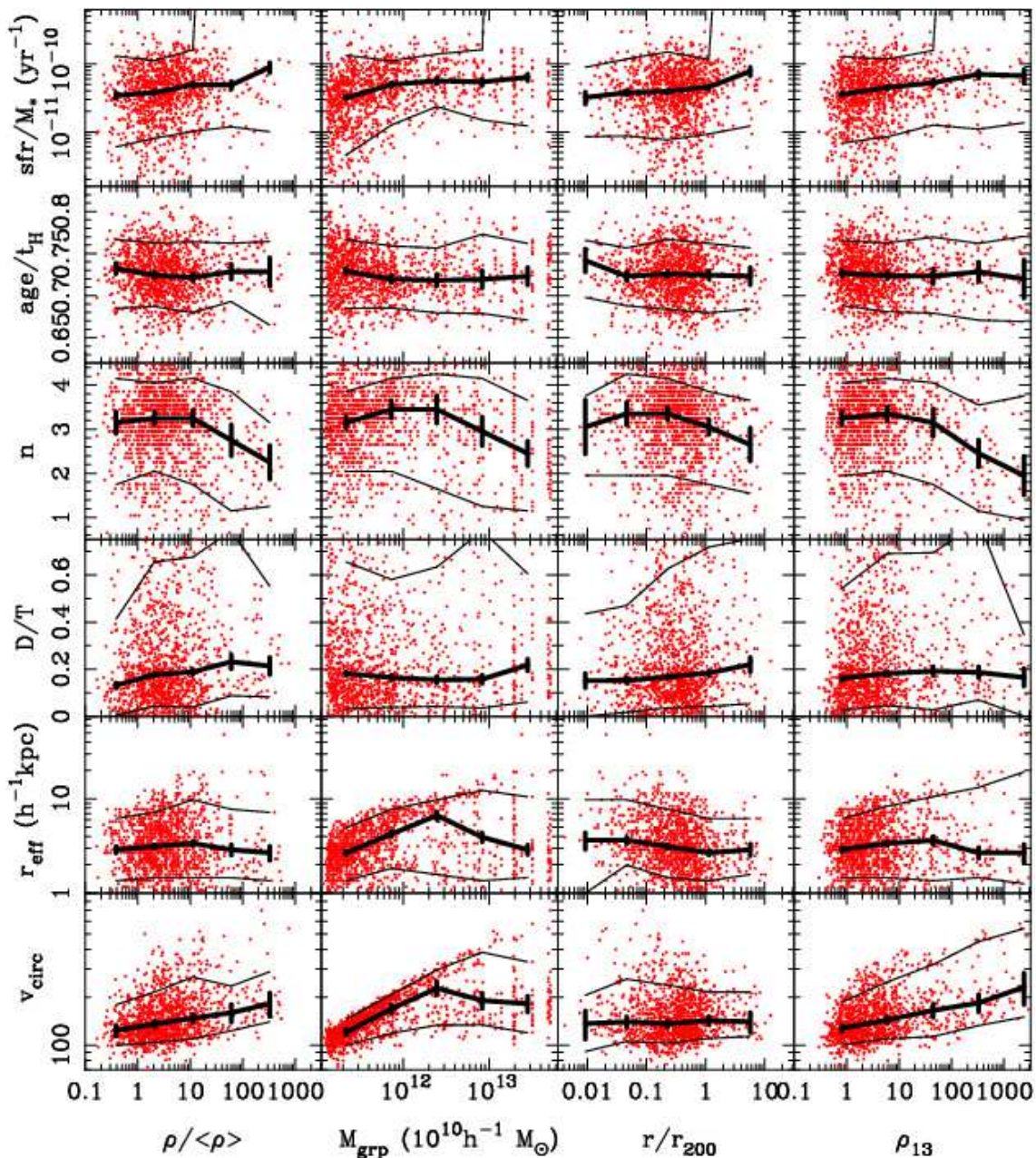


Figure 12. Galaxy properties versus environment at $z = 1$ in the *BHCosmo* simulation. The measures of environment are, from left to right, galaxy density (measured from the distance to the 10th nearest neighbour galaxy) in units of the mean, mass of the host friends-of-friends group, distance from the center of mass of the friends-of-friends galaxy, in units of the virial radius, r_{200} , and dark matter density computed from the radius which encloses $10^{13}h^{-1}M_{\odot}$ of dark matter. In each panel, results for individual galaxies are shown as points, and the median is shown as a thick solid line with Poisson error bars. The 90th and 10th percentiles of the distribution in each bin are shown as thin solid lines.

simulation box, at $33.75 h^{-1}\text{Mpc}$ is too small to contain any clusters at $z = 1$. Cooper et al. (2007) have investigated the observed relationship between galaxy color and local density from redshifts $z = 0.4$ to $z = 1.35$, finding that the trend of red sequence galaxies to favour overdense regions evolves strongly over that redshift range. The locations of red galaxies $z \sim 1$ are however still seen to correlate with high densities. Population synthesis models will be needed to compare colors of our simulated galaxies with this information. For now, we restrict ourselves to the morphological

information we have computed, although as we shall see in the next section, the morphology-density relation in the simulation also appears to evolve somewhat more weakly than in the observations.

4.3 Morphology-density relation

The tendency of dense (galaxy cluster) environments in the low redshift Universe to contain a higher fraction of early types than the field has long been known (Dressler 1980).

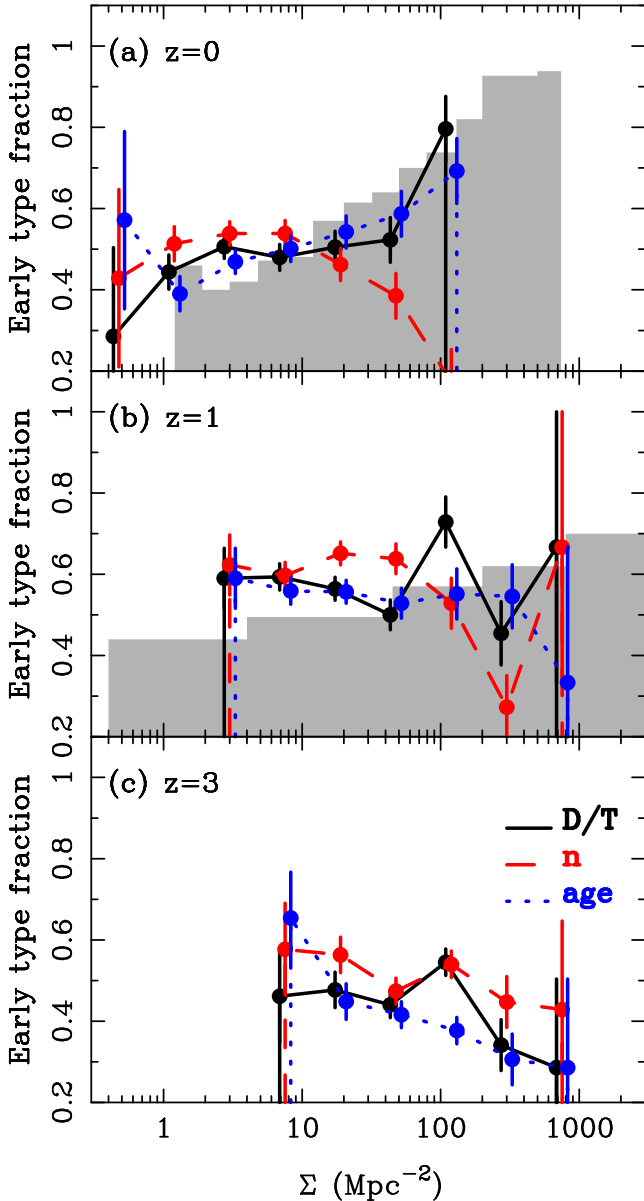


Figure 13. The morphology-density relation at 3 redshifts. We show as different lines results for galaxies types selected on the basis of kinematic D/T ratio, Sersic index, and mean stellar age (see text). The x -axis, Σ is the projected galaxy density. Panels for $z = 1$ and $z = 3$ are for galaxies from the *BHcosmo* simulation, and $z = 0$ galaxies are taken from the D4 run. As shaded histograms in the top 2 panels we show the observational results of Dressler (1980,1997) at $z \sim 0$ and Smith et al. (2005) at $z = 1$.

Recently it has become possible to extend this work to higher redshifts, $z = 0.5 - 1$ and beyond. Here we compare simulation results for this morphology-density relation to the observational data of Smith et al. (2005), which, along with data from $z = 0.75 - 1.27$ includes a compilation at lower and intermediate redshifts from Dressler (1980, 1997), and Treu et al. (2003).

The galaxies in the Smith et al. sample and compilation have limiting V magnitude of -20.2 at $z = 0$ (-21.2 at $z=1$). Their space density (using the luminosity function of Brown

et al. 2001) is $5.12 \times 10^{-2} (h^{-1} \text{Mpc})^{-3}$ at $z=0$. The observational fraction of early-type galaxies is plotted as a function of projected galaxy density at 2 different redshifts in the top 2 panels of Figure 13. The projected galaxy density is the density enclosed within a rectangular region extending to the 10th nearest galaxy. In order to include redshift information in the $z = 1$ data, Smith et al. include galaxies in the density estimate in slices of redshift width $\Delta z = 0.1$. They also subtract a background galaxy density from the density estimate and also multiply by a density correction factor of 2. After this procedure, their results are that the correlation between early type fraction and density is still present at $z = 1$, but significantly weaker than at $z = 0$ (and also $z = 0.5$, which lies in between, and is not plotted here).

In order to make predictions from the simulations, we also compute a projected galaxy density measured from the area delimited by the 10th nearest neighbor. It is not possible to replicate entirely the relatively involved procedure employed by Smith et al. , but we make sure that we are centered on the same mean projected galaxy density, and make sure that our results are robust by also trying a completely different density estimator, as explained below.

We project the whole simulation box, using information from the 3 different orthogonal projections in our data sample. This results in a lower mean projected galaxy density than Smith et al. , who at $z = 1$ have a mean area density of galaxies of 5.25 per Mpc^2 . Our galaxy density is 2.0 per Mpc^2 , so that we correct our projected simulation density values by a constant factor to bring them into agreement. This is under the assumption that the overdensity of galaxies relative to the mean is the physically relevant quantity. We have also tried computing the morphology density relation using the 3 dimensional galaxy overdensity from the simulations, for comparison. We find that all the qualitative conclusions we draw from the comparison with projected observational data also hold, giving us confidence in the robustness of the results.

In order to find the early type fraction, we compute three different values using three different criteria, kinematic D/T ratio, Sersic index and age. For the kinematic selection, we use a cutoff of $D/T=0.2$ between early and late types, and for the Sersic index, a threshold of $n = 3.0$, For the age criterion, we used a cutoff mean stellar formation redshift between early and late types which is different for the 3 redshift bins ($z = 0.0, 1.0$ and $z = 3.0$) we use. In order to set the threshold, we choose values which make the overall fraction of early and late types the same as for our D/T ratio criterion. This cutoff stellar formation redshift is $z = 2.6, 3.8$ and 4.8 for redshift bins $z = 0, 1.0$ and $z = 3.0$ respectively.

Our results for the morphology-density relation in the simulations are shown in Figure 13 alongside the observational results at $z = 0$ and $z = 1$. We also show the simulation predictions for redshift $z = 3$. We can see that at $z = 0$, the early type fraction increases in high density regions. Although there are no rich clusters in our relatively small volume, the simulation curves with early types selected kinematically by and age track reasonably well the observational results up to moderate galaxy density. The photometric criterion however diverges at the high end of the density range, with the number of galaxies with $n > 3$ falling dramatically at projected densities $> 20 \text{Mpc}^{-2}$. This behaviour was also seen in Figure 12.

At redshift $z = 1$, the morphology-density relation in the simulation flattens out, with no increase seen in the fraction of early types at high densities in the middle panel of Figure 13. This change between $z = 0$ and $z = 1$ is somewhat more extreme than that which is seen observationally, although the sign of the change is the same. Again the selection by Sersic index gives the most discrepant results. At $z = 3$, the simulations predict a complete reversal of the morphology density relation, with the fraction of galaxies with younger stellar populations being highest in the densest regions. It is to be noted that because the units of the x -axis of Figure 13 are in proper Mpc, the galaxy density of the different redshift samples is affected by the expansion of the universe.

Because the simulation volume is relatively small, we are restricted to computing the morphology-density relation for galaxies with a relatively small range of stellar masses (there are few extremely massive galaxies for example, particularly at $z = 1$ and above). Recently, it has been found (F. van den Bosch, private communication, Weinmann et al. 2008) that for (satellite) galaxies in a fixed stellar mass bin, there is no significant morphology dependence on host halo mass, i.e. observationally the morphology-density relation seems to be driven by the stellar mass-density relation. The results we find in the simulation for the morphology-density relation could be therefore be relatively flat at least partly because of our small range of galaxy masses. We note that we have accounted for differences between central and satellite galaxies in our study, whereas Weinmann et al. find that their result holds for satellite galaxies only. Larger simulations will be needed to investigate conclusively whether the morphology-density relation in simulations is flat for bins of galaxy stellar mass.

We have seen that the morphology-density relation flattens out or inverts at higher redshifts. However, what is not easily seen in Figure 13 is that the overall fraction of early type galaxies change with redshift as well. We have applied the same thresholds to separate early and late types ($D/T > 0.2$ and $n < 3.0$ for late types) in outputs of the *BHCosmo* run at redshifts up to $z = 9$. The results are shown in Figure 14, where we can see that the two means of separating galaxy types do agree at $z = 4$ and below. At high redshifts, although the errors are large, the correspondence between type chosen through D/T and n is not good, with galaxies appearing to become steeper of profile but at the same time having smaller kinematically defined bulges. Based on the resolution tests (Figure 5), D/T is likely to be a more robust discriminator between galaxy types. This conclusion is understandable if we take into account the fact that single component Sersic profiles are often not a good characterization of the profile shape of post-starburst ellipticals, as found by Hopkins et al. (2008) and discussed further in Section 3.4.

At lower redshifts, however, the number of early types does increase significantly. As described by D/T ratio, the early type fraction increases from ~ 0.35 at $z \sim 9$ to ~ 0.6 at $z = 1$. The early types chosen by n also increase below $z = 4$. Following galaxy properties in detail with redshift is beyond the scope of this paper, so we will confine ourselves to noting that the general decrease in the fraction of disk galaxies as the universe evolves seen here is the same qualitative trend seen observationally (e.g., Postman et al. 2005).

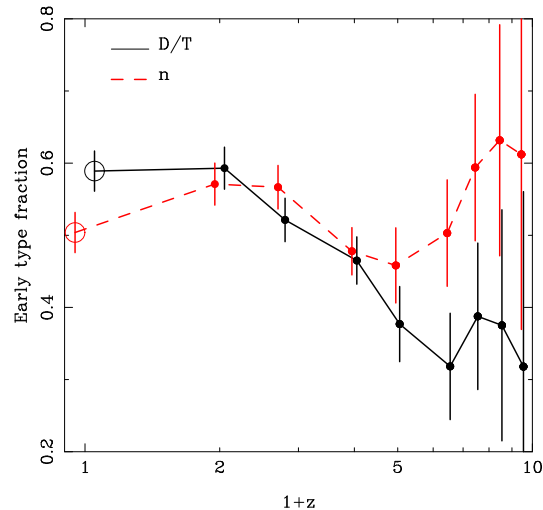


Figure 14. The early-type fraction of simulated galaxies as a function of redshift. Galaxies were classified either on the basis of kinematic D/T ratio (> 0.2 for late type) or Sersic index, ($n < 3.0$ for late type), as in Figure 13). The filled points (i.e. $z \geq 1$) are for the *BHCosmo* simulation and the open points for the D4 run.

5 LARGE-SCALE STRUCTURE AND CLUSTERING

The galaxies in our simulations form at the same time as the cosmic web of large-scale structure. We have seen from the previous section how the local environment of galaxies affects their properties. We will now turn to larger scales, examining the morphology of this structure as traced by different types of galaxies and also their clustering, measured using the autocorrelations function. As with the previous section, the relatively small simulation volume means that we will not have instances of truly rare events, rich clusters of galaxies, and also the box size will have some effect on the overall amplitude of clustering. For this reason, we will concentrate on the differences between dark matter and galaxy clustering, their relative bias, for different galaxy types. This should be less sensitive to the small box size than the raw amplitude of the autocorrelation function (following the approach of e.g., Katz et al. 1999).

5.1 Visual impression

In Figure 15 we show $10 h^{-1}$ Mpc thick slices through the galaxy and dark matter density fields, at 3 different redshifts. We have used our usual D/T threshold of 0.2 to classify galaxies into early and late types, which are plotted using different symbols. The same 5000 particle lower limit for subhalos is again used at all redshifts, except for the left-most panel, which is taken from the D4 run. In this case, we use the equivalent particle limit, scaled from the *BHCosmo* run using the ratio of mass resolutions.

Looking at the three different redshift panels, the overall framework of structures looks quite similar at different times. In the dark matter plots, the dense regions at $z = 3$, are quite web-like, made up of many intersecting filaments, whereas at $z = 0$ they have collapsed into more compact structures. On larger scales, however, not much appears to

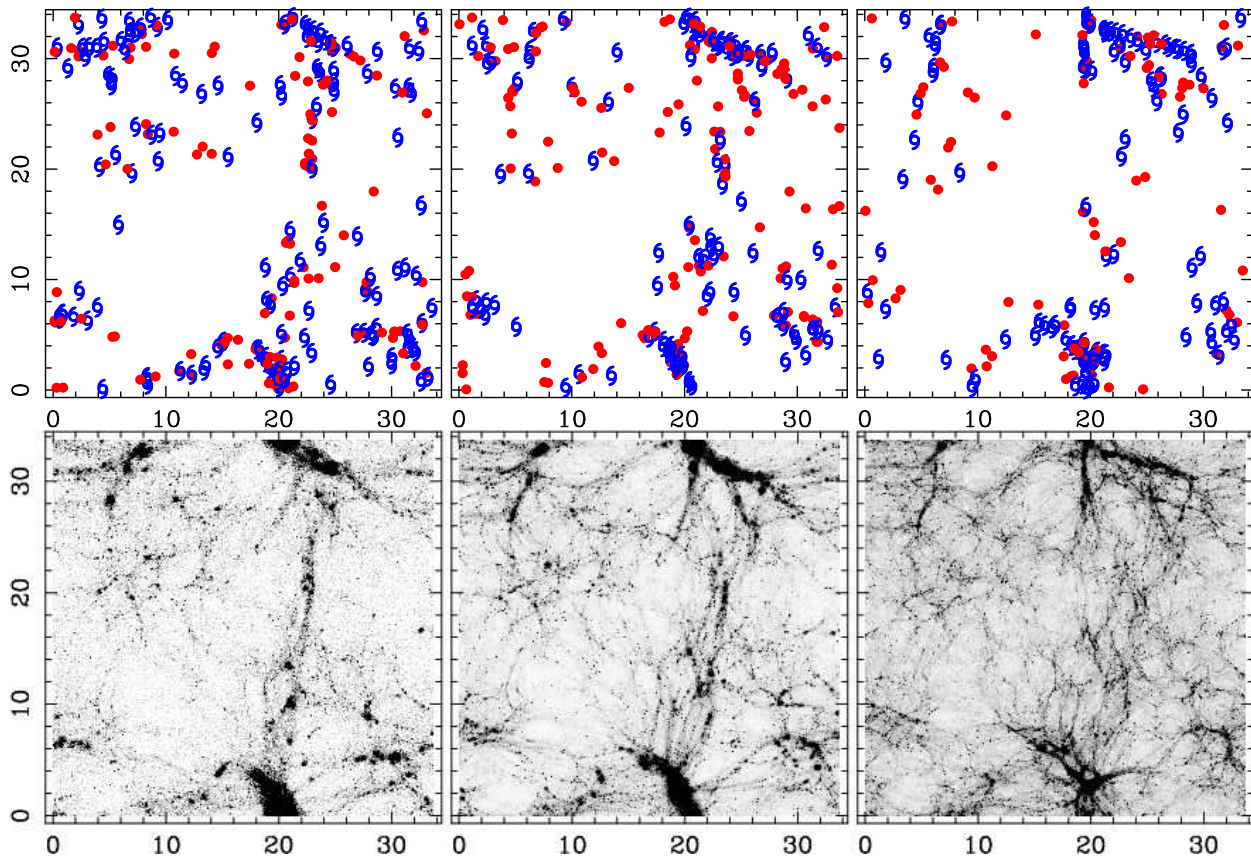


Figure 15. Large-scale structure in the galaxy and dark matter distribution. Top row: slices ($10 h^{-1}\text{Mpc}$ thick) through the simulated galaxy distributions at 3 redshifts. Late type galaxies (selected so that $D/T > 0.2$) are shown as spiral symbols and early types as points. The leftmost panel, $z = 0$ is for the D4 simulation, and the two right panels ($z = 1$, middle and $z = 3$, right) are from the *BHCosmo* run. Bottom row: a linear greyscale plot of the dark matter distribution in the same regions of the same simulations shown in the top row.

have changed, particularly when looking at the galaxy distribution.

Comparing the distribution of early and late types, we see some evidence for dense clumps of early types at $z = 0$ (for example at the bottom of the panel). There may also be marginally more late types around the outskirts of these structures, although the situation does not look markedly different at higher redshift. At redshifts 1 and 3, however there do seem to be many early types which are relatively isolated, somewhat more than late types. More conventionally, the protogroup of the bottom of the panel appears at redshift 3 to consist of more late types, and then at $z = 0$ it collapses into a virialized group of early types. Apart from this, however the visual impression at $z = 1$ and above is that late types are marginally more highly clustered in the simulation. We shall see below that this is borne out by quantitative measurement.

5.2 The autocorrelation function

We use the same delimitations between galaxy types as in Figure 13 to investigate the autocorrelation function of early and late types. We look at three redshifts, $z = 3$, $z = 1$ and $z = 0$, using the D4 simulation for the latter. In addition, we separate the full sample into two sets, by mass, in order to see whether the mass dependence has a larger effect on clus-

tering. In order to compare the results directly with those of galaxy types, we chose to make the higher mass subsample in each case have the same number of galaxies as those with $D/T < 0.2$.

We compute $\xi(r)$ in real space, making use of the periodic boundary conditions of the simulation. The results are shown in Figure 16. Also given in each panel are values for the large-scale bias between galaxies and dark matter. For the early types it is computed using $b_E = \sqrt{\xi_E/\xi_{dm}}$ and analogously for the late types. We also compute the bias for the high mass and low mass subsamples. In each case we give the mean value for the 5 bins between $2 h^{-1}\text{Mpc}$ and $10 h^{-1}\text{Mpc}$, and an error which comes from the standard deviation of the results for the 5 bins.

On scales $r \gtrsim 1 h^{-1}\text{Mpc}$ we can see that in all panels we have approximately scale independent bias between galaxies and dark matter. All galaxy subsamples at $z \geq 1$ have a higher amplitude of clustering on these scales than the dark matter, with the lowest amplitude corresponding to $b = 1.08 \pm 0.03$. At redshift $z = 3$, this bias can be as high as $b = 2.48 \pm 0.12$, so that the galaxies follow the familiar “high peaks” biasing trend where similar mass galaxies at higher redshifts are associated with rarer, higher peaks and are biased more strongly (e.g., Bardeen et al. 1986). The values of bias decrease until at $z = 0$, all galaxies are antibiased with respect to the dark matter.

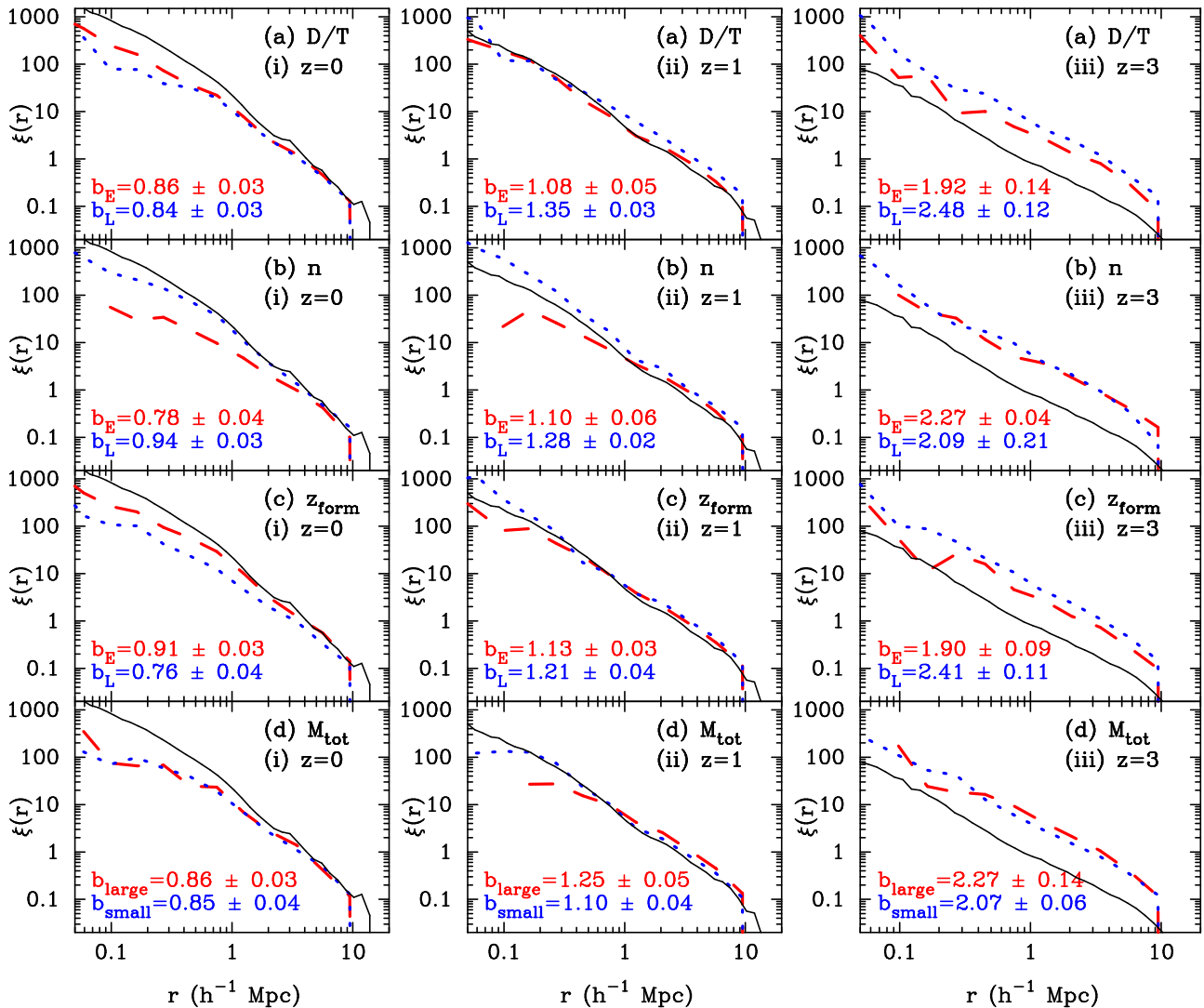


Figure 16. The autocorrelation function of simulated galaxies as a function of type and redshift. The 3 columns show results for $z = 0$, $z = 1$ and $z = 3$, from left to right, with the $z = 0$ results taken from the D4 simulation and the rest the *BHCosmo* run. In each row, (a)-(c) we show galaxies classified into early and late types by D/T ratio, Sersic index and mean stellar age. In row (d), we show results for galaxies split into two mass classes (see text). The galaxy correlation function results are shown as dotted lines for late types (and low mass, “small” galaxies in row (d)) and dashed lines for early types. In each panel we also plot the autocorrelation function of the dark matter as a thin solid line. The bias factor between the dark matter and the galaxies is given in each panel, computed from the average of the bias factor in the 5 bins with $10 h^{-1}\text{Mpc} > r > 2 h^{-1}\text{Mpc}$. The quoted 1σ errors are derived from the standard deviation of results for the 5 bins.

The subsamples based on mass also act in the fashion expected from high peaks theory, with the more massive galaxies being more biased. However, if we look at the different methods for classifying types, we can see that in many cases the late types are more highly biased than the early types. At $z \geq 1$, no matter how galaxies are classified, the late types are more highly biased. The largest difference is for the kinematic classification, at $z = 1$ for which high D/T galaxies are 25% more biased. Even for galaxies classified based on mean stellar age we see this trend, with the youngest galaxies (assumed to be late types) being 7% more biased at this redshift.

We therefore find that at high redshifts, the disk galaxies have a higher correlation function ($b = 1.35 \pm 0.03$ at $z = 1$) on large scales than the high mass galaxy subsam-

ple ($b = 1.25 \pm 0.05$ at $z = 1$), even though they actually have a lower median circular velocity ($v_{\text{circ}} = 136 \text{ km s}^{-1}$ vs $v_{\text{circ}} = 177 \text{ km s}^{-1}$). This is quite interesting, implying that the processes which determine whether a galaxy is an early or late type at these redshifts are even more closely coupled to clustering than galaxy mass.

At redshift zero, the situation reverses itself for the most part, with early types chosen on the basis of D/T and mean stellar age being more clustered than the late types. The difference in the clustering of the large and small mass subsets also becomes statistically insignificant.

If we now turn to small scales $r \lesssim 1 h^{-1}\text{Mpc}$, the clustering between galaxies and mass does become scale-dependent. Selecting galaxy type using n changes the amplitude the most, with early types being a factor of ~ 20

times more clustered at a separation of $r = 0.1 h^{-1}\text{Mpc}$ at $z \leq 1$. This can be compared with the D/T plot, for which kinematic separation has little effect on ξ . The difference in the slope of the stellar profile fitted for galaxies with different n therefore has effects on much larger scales than individual galaxies. Given that the effects of galaxy exclusion are seen in the large mass subsample at $z = 1$ (ξ_{large} drops to zero at radii presumably close to twice the radius of large galaxies), one might worry that this is also happening in the n panel. However, looking at Figure 6 one can see that galaxies with $n > 3$ essentially sample the entire V_{circ} range, so this is unlikely to be a problem.

Observationally, several recent studies have begun to probe the details of clustering as a function of galaxy properties at redshift $z = 1$. For example, Coil et al. (2006) have investigated luminosity dependence of clustering in the DEEP2 redshift survey, finding that more luminous galaxies are more strongly clustered than fainter ones, with the dependence of relative bias on luminosity being even stronger at $z = 1$ than $z = 0$. For a concordance cosmology, the bias seen by Coil et al. varies from $b = 1.26 - 1.54$. The number density of galaxies for the observed sample with the lowest luminosity threshold is $1.3 \times 10^{-2} (h^{-1}\text{Mpc})^{-3}$, within 10% of the space density of our simulation sample of “large” galaxies plotted in panel (d) of Figure 16. The observed value of the bias from Coil et al. is $b = 1.26 \pm 0.04$, compared to our simulation value of $b_{\text{large}} = 1.25 \pm 0.05$. The observed clustering amplitude for a given space density therefore appears to be reproduced by the simulations. We note that in this comparison, the bias measured by Coil et al. is the linear bias whereas we measure the bias with respect to the non-linear dark matter. At this relatively high redshift and on the scales we measure we do not expect there to be a significant difference. We leave the investigation of clustering as a function of luminosity and color and exploration of results for higher redshifts (where the simulation bias predictions are much higher) to future work.

Meneux et al. (2008) have carried out a detailed study of clustering of galaxies as a function of stellar mass at $z \sim 1$ (actually $z = 0.85$ mean redshift) in the VIMOS-VLT Deep Survey. This can be compared directly to our simulation results. To do this, we have split up our $z = 1$ sample into the same stellar mass bins as Meneux et al. . These are $\log(M/M_{\odot}) = 9.5 - 10.0$, $\log(M/M_{\odot}) = 10.0 - 10.5$, and $\log(M/M_{\odot}) = 10.5 - 11.0$. Meneux et al. find a bias of 1.29 ± 0.10 , 1.32 ± 0.10 and 1.62 ± 0.18 for these three bins, respectively. Our results are 0.86 ± 0.05 , 1.05 ± 0.03 and 1.30 ± 0.07 . Compared to this sample of galaxies, our clustering results are therefore somewhat lower. This could be understood if the stellar masses of our simulated galaxies are higher for a given space density than in the observations. Another possibility is that the relatively small box size of the simulation (with the fundamental mode of the box going mildly non-linear at $z = 1$) is affecting the result. As we mentioned above, this should be less of a problem for the prediction of the relative bias between dark matter and galaxies than for the raw galaxy ξ , but should still be borne in mind. We leave further investigation of the mass function by stellar mass of the simulated galaxies to future work.

The clustering of DEEP2 galaxies around SDSS quasars has been measured by Coil et al. (2007), who find from the cross correlation that they are distributed similarly, with

no dependence on scale, quasar luminosity or redshift. In the future, the *BHcosmo* simulation can be used to compare to these observations in detail. For now we note that some qualitatively similar findings (limited dependence of quasar properties on environment) has been found in the simulation by Colberg & Di Matteo (2008).

6 SUMMARY AND DISCUSSION

6.1 Summary

We have examined the galaxies forming in a cosmological hydrodynamic simulation which includes self consistent modelling of black hole growth and feedback. The mass and spatial resolution of the simulation are similar to those of previous zoomed simulations of individual galaxies, enabling us to explore to a similar accuracy the properties of a population of ~ 1000 galaxies with circular velocities $\gtrsim 100 \text{ km s}^{-1}$. Our conclusions can be summarised as follows.

(1) At redshift $z = 1$ we find that galaxies can be roughly divided into classes on the basis of their morphology, kinematics and age. These can be associated with the classic division into “early” and “late” types, so that on average most of the usually assumed relationships between galaxy properties hold. These relationships are that smaller galaxies tend to be younger, have smaller Sersic indices, higher kinematic disk to bulge ratios and star formation rates than older, larger galaxies.

(2) The angular momentum content of galaxies (compared to observations) is still a problem, as it is for the zoomed simulations. We find that disk galaxies in the simulation have on average ~ 8 times less specific angular momentum for a given circular velocity than in the observational compilation of Navarro (1998). The kinematic decomposition of galaxies into disk and bulge fraction also leads to a much higher proportion of bulge dominated galaxies than in observations. The inclusion of black hole physics does not appear to alleviate the angular problem (also found in the zoomed simulations of Okamoto et al. 2007).

(3) The scale length of disk galaxies for a given circular velocity is approximately consistent with observations. The flattened parts of galaxies are therefore partially supported by non-circular motions. This is related to the fact that the simulated disk galaxies also compare acceptably to the $z = 1$ stellar mass Tully-Fisher relation observations of Kassin et al. (2007), who include a non-circular component (gas velocity dispersion) in their preferred statistic. When computing the same statistic for the simulations, the overall agreement is acceptable, but with a different ratio of rotational and non-rotational motions than the observations. The extended stellar populations of galaxies are approximately the right size, but are kinematically distributed differently.

(4) The properties of galaxies in the simulation are related to their large scale environment, in a fashion which changes with redshift. At $z = 0$, the higher fraction of early types in dense environments is qualitatively similar to that seen in observational data (e.g., Dressler 1980). At higher redshifts, the observational and simulation trends are both for relatively more late types at high densities. However, the simulation predicts somewhat too many, with an actual reversal of the morphology density relation.

(5) The overall fraction of disk (late type) galaxies in the simulation decreases as we move to lower redshifts, changing from > 0.7 at $z \sim 10$ to ~ 0.45 at $z = 0$.

(6) The clustering of galaxies (with $v_{\text{circ}} > 100 \text{ km s}^{-1}$) is slightly stronger than that of the dark matter, with the correlation function $\xi(r)$ exhibiting an average positive bias factor $b \sim 1.2$ on scales $r > 0.5 h^{-1} \text{ Mpc}$. At $z = 1$, we find that late type galaxies (selected by either age, kinematics or Sersic index) are actually more positively biased than early types, a reversal of the trend observed at low redshifts.

6.2 Discussion

As with previous zoomed simulations of disk galaxies, our results are mixed. There are many aspects of the simulated galaxies which agree qualitatively and quantitatively with observational data, but there are also still important differences. The large fraction of mass in bulge components, linked to the lack of orbital stellar angular momentum are the most obvious. In order to form more realistic disk galaxies in this type of simulation, it is likely that subtleties in the feedback mechanisms need to be changed. Okamoto et al. (2005) have investigated different models of feedback in zoomed simulations, finding that galaxy morphologies are extremely sensitive to how the feedback is applied and how it is related to star formation. For example, they find that when star formation is formed through shock induced compression of gas (a “burst” mode), the feedback heats up a large reservoir of gas which later cools to form an extended rotationally supported disk. On the other hand, Okamoto et al. (2005) find that concentrating injection of feedback energy in high density regions (a rough approximation of AGN feedback) does not have the same effect. We have seen in this paper (as Okamoto et al. 2007 also did with zoomed simulations with black holes) that modelling AGN feedback with black hole particles does indeed not solve the angular momentum problem. Clearly, different models of feedback should be explored in simulations which encompass a fair sample of galaxies. In the present work, we have shown that the multiphase model for star formation of Springel & Hernquist (2003) can be used to simulate galaxies in a uniform cosmological run with the same relative degree of success as in the zoomed runs of Robertson et al. (2004).

Numerical and algorithmic issues can also influence the morphology of galaxies as well as implementations of feedback physics. For example, Governato et al. (2007) have found that increasing numerical resolution has led to some improvement in the rotational support of disks and less transfer of angular momentum to the dark matter. We have seen in the present paper that our low resolution D4 run is not very much different than the *BHCosmo* run, so that it seems unlikely that straightforward decreases in particle mass and gravitational softening length would result in significantly better agreement with observations than could be obtained without also changing the way star formation and feedback are modelled. In the present work, we have made use of multiphase modelling of subresolution star formation physics which Springel & Hernquist (2003b) have shown exhibits good convergence properties. However, better modelling of star formation and less dependence on subresolution parametrization would go hand in hand with increased resolution. For example, Pelupessy et al. (2006) find that

explicit modelling of molecular hydrogen formation in SPH simulations of dwarf galaxies requires gravitational softening on the order of tens of pc and gas particle masses of $\sim 10^3 h^{-1} M_{\odot}$. Ceverino & Klypin (2007) have recently shown with AMR simulations of hot gas bubbles caused by star formation that modelling these bubbles self consistently without subresolution assumptions requires 50pc resolution.

On the algorithmic side, there is the possibility that issues with SPH are affecting the gas physics that can be modelled well. For example, Agertz et al. (2007) have recently shown that spurious pressure forces on particles can arise in regions where there are steep density gradients (but see Price, 2007 for natural ways to resolve this within the SPH formalism). On the other hand, Bryan (2007) has shown that the overly centrally concentrated density distributions and rotation curves that are a generic feature of simulations of spiral galaxies also occur in extremely high resolution simulations of disks using Adaptive Mesh Refinement. Bryan (2007) concludes that more sophisticated modelling of the interstellar medium, including star formation and turbulent support is needed to resolve these issues in galaxy formation.

Some of the results in this paper may have a slightly different interpretation if the classification of early and late type galaxies is broadened into more categories. For example, dwarf ellipticals and their subtype dwarf spheroidals are known to have many of the properties of spiral galaxies rather than larger ellipticals (e.g., Grebel et al. 2003). It is possible that some of the effects we are seeing are partly due to this (for example the higher clustering amplitude of late types at high z could partially be because there are many dwarf galaxies in the early type sample). Our lower cutoff in mass corresponds to a circular velocity $\sim 100 \text{ km s}^{-1}$, probably too high for most true dwarfs, but still low enough that these possibilities should be investigated further in future work. It is also possible that irregular galaxies and their properties could be investigated separately. Future work at higher resolution will eventually make this possible.

The presence of late-type galaxies at high redshifts in high density environments which we have seen in §4.3 in the *BHCosmo* simulation has long been seen observationally. For example, clusters at $z > 0.4$ contain substantial populations of blue spiral galaxies (e.g., Butcher and Oemler 1978) which evolve much more rapidly than field galaxies in the 4-5 Gyr timescale to $z = 0$. Transformation of these galaxies by “galaxy harassment” (Moore et al. 1996) into dwarf ellipticals may be ongoing in our simulation, and partially account for the rising fraction of early types at lower redshifts. We can see from the morphology-density relation in Figure 13 that there is indeed much more evolution of the galaxy population at the high density end.

Van den Bosch et al. (2007) have investigated the morphological transformations that take place in high density environments in the SDSS, looking at the difference between central and satellite galaxies. They find that whenever a central galaxy falls into a bigger halo (i.e., becomes a satellite), it undergoes a color change (becoming slightly redder) and a morphology change (becoming very slightly more concentrated). They find that the magnitude of this effect is independent of the mass of the new host halo in which the galaxy falls. This suggests that ram-pressure stripping of cold gas is not the likely cause, but instead “strangulation”, or removal of the galaxy halo hot gas. This takes place over a relatively

long timescale (not accounted for in past semi-analytic models, as shown by Kang & van den Bosch (2008)). In our simulation, we do find in Figure 12 that galaxies become more centrally concentrated (n increases) as a function of decreasing distance from the host halo center. Tracking the role of gas accretion and loss from the galaxies (as carried out by e.g., Kereš et al. 2005) could be used to investigate the mechanism by which this occurs.

Much of the focus of galaxy formation simulations has been on trying to form realistic disks. We have seen in the present work that we are able to achieve a similar degree of success (for example in the specific angular momentum-circular velocity relationship) in our full volume cosmological run to earlier zoomed simulations (e.g., Robertson et al. 2004, Abadi et al. 2003ab). We have not looked in so much detail however at the elliptical galaxies formed in the *BH-Cosmo*. Naab et al. (2007) have recently performed zoomed simulations of early-type galaxies from Λ CDM initial and find that realistic intermediate mass elliptical galaxies can be formed even without recent major mergers or AGN and supernova feedback. We have mass resolution throughout our box only ~ 3 times worse, than in the fiducial zoomed runs of Naab et al. (although we have significantly coarser spatial resolution), so that it would be worth investigating the properties of the larger population of early types in more detail in future work.

In the future, it will be necessary to run a larger box down to redshift $z = 0$. In this way, it will be possible to investigate a wider range of environments, including rich clusters, where the evolutionary history of simulated galaxies is expected to be different from galaxy groups and the field. A much wider range of observational data is also available at $z = 0$. Population synthesis modelling of the simulated galaxies would enable more direct comparisons with the data, including the effect of observing in different wavelengths on morphology.

ACKNOWLEDGMENTS

We thank Jörg Colberg for providing the subhalo files and Jörg Colberg and Andrew Zentner for useful discussions. This work was partially supported by the National Science Foundation, NSF AST-0205978 and NSF AST-0607819. The simulations were carried out at Carnegie Mellon University and on the Cray XT-3 at the Pittsburgh Supercomputing Center.

REFERENCES

- Abadi, M. G., Navarro, J. F., Steinmetz, M., Eke, V. R., 2003a, *ApJ*, 591, 499
- Abadi, M. G., Navarro, J. F., Steinmetz, M., Eke, V. R., 2003b, *ApJ*, 597, 21
- Agertz, O., Moore, B., Stadel, J., Potter, D., Miniati, F., Read, J., Mayer, L., Gawryszczak, A., Kravtsov, A., Nordlund, Å., Pearce, F., Quilis, V., Rudd, D., Springel, V., Stone, J., Tasker, E., Teyssier, R., Wadsley, J. and Walder, R., 2007, *MNRAS*, 380, 963
- Bailin, J. & Steinmetz, M., 2005, *ApJ*, 627, 647
- Bardeen, J. M., Bond, J. R., Kaiser, N. & Szalay, A. S., 1986, *ApJ*, 304, 15
- Bell, E. F.; Wolf, C., Meisenheimer, K., Rix, H.-W., Borch, A., Dye, S., Kleinheinrich, M., Wisotzki, L., & McIntosh, D. H., 2004, *ApJ*608, 752.
- Blanton, M. R., Eisenstein, D., Hogg, D. W., Schlegel, D. J. and Brinkmann, J., 2005, *ApJ*, 629, 143
- Blanton, M. R., Hogg, D. W., Bahcall, N. A., Baldry, I. K., Brinkmann, J., Csabai, I., Eisenstein, D., Fukugita, G., Gunn, J. E., Ivezić, Z., Lamb, D. Q., Lupton, R. H., Loveday, J., Munn, J. A., Nichol, R. C., Okamura, S., Schlegel, D. J., Shimasaku, K., Strauss, M. A., Vogeley, M. S. & Weinberg, D. H., 2003, *ApJ*, 594, 186
- Brown, W., R., Geller, M.J., Fabricant, D.G., & Kurtz, M.J., 2001, *AJ*, 122, 714
- Butcher, H. & Oemler, A, 1978, *ApJ*, 219, 18
- Capak, P., Abraham, R. G., Ellis, R. S., Mobasher, B., Scoville, N., Sheth, K. and Koekemoer, A., 2007, *ApJ-Supp.*, 172, 284
- Ceverino, D., & Klypin, A., *ApJ*submitted, arXiv:0712.3285v1 [astro-ph]
- Coil, A. L., Newman, J. A., Cooper, M. C., Davis, M., Faber, S. M., Koo, D. C., Wilmer, C.N.A., 2006, *ApJ*, 644, 671
- Coil, A.L., Hennawi, J. F., Newman, J. A., Cooper, M. C. & Davis, M., 2007, *ApJ*, 654, 115
- Coil, A. L., Newman, J. A., Croton, D., Cooper, M. C., Davis, M., Faber, S. M., Gerke, B. F., Koo, D. C., Padmanabhan, N., Wechsler, R. H. & Weiner, B. J., 2008, *ApJ*, 672, 153
- Colberg, J.M., & Di Matteo, T., 2008, *ApJ*, submitted
- Cooper, M. C., Newman, J. A., Coil, A. L., Croton, D. J., Gerke, B. F., Yan, R., Davis, M., Faber, S. M., Guhathakurta, P., Koo, D. C., Weiner, B. J. and Willmer, C. N. A., 2007, *MNRAS*, 376, 1445
- Cooper, M. C. and Newman, J. A. and Weiner, B. J. and Yan, R. and Willmer, C. N. A. and Bundy, K. and Coil, A. L. and Conselice, C. J. and Davis, M. and Faber, S. M. and Gerke, B. F. and Guhathakurta, P. and Koo, D. C. and Noeske, K. G., 2008, *MNRAS*, 383, 1058
- Courteau, S., 1997, *AJ*, 114, 2402
- Croton, D., J., Springel, V., White, S. D. M., De Lucia, G., Frenk, C. S., Gao, L., Jenkins, A., Kauffmann, G., Navarro, J. F. & Yoshida, N., 2006, *MNRAS*, 365, 11
- Dalcanton, J. J. & Bernstein, R.A., 2000, *AJ*, 120, 203
- Di Matteo, T., Springel, V., and Hernquist, L., 2005, *Nature*, 433, 604
- Di Matteo, T., Colberg, J., Springel, V., Hernquist, L., & Sijacki, Debora, 2007, *ApJ*, in press, arXiv:0705.2269
- Dressler, A., 1980, *ApJ*, 236, 35
- Dressler, A., Oemler, A. J., Couch, W. J., Smail, I., Ellis, R. S., Barger, A., Butcher, H., Poggianti, B. M. and Sharples, R. M., 1997, *ApJ*, 490, 577
- Evrard, A. E., 1988, *MNRAS*, 235, 911
- sph1 Gingold, R. A. & Monaghan, J. J., 1977, *MNRAS*, 181, 375
- Governato, F., Mayer, L., Wadsley, J., Gardner, J. P., Willman, Beth, Hayashi, E., Quinn, T., Stadel, J. & Lake, G., 2004, *ApJ*, 607, 688
- Gómez, P. L., Nichol, R. C., Miller, C. J., Balogh, M. L., Goto, T., Zabludoff, A. I., Romer, A. K., Bernardi, M., Sheth, R., Hopkins, A. M., Castander, F. J., Connolly,

- A. J. , Schneider, D. P. , Brinkmann, J. , Lamb, D. Q. , SubbaRao, M. and York, D. G., 2003, *ApJ*, 584, 210.
- Governato, F., Willman, B., Mayer, L., Brooks, A., Stinson, G. , Valenzuela, O., Wadsley, J. and Quinn, T., 2007, *MNRAS*, 374, 1479
- Graham, A., 2001, *AJ*, 121, 820
- Grebel, E. K., Gallagher, J. S., III, Harbeck, D., 2003, *AJ*, 125, 1926
- Hernquist, L. & Katz, N., 1989, *ApJSupp.*, 70, 419
- Hopkins, P.F., Hernquist, L., Cox, T.J., Dutta, S., & Rothberg, B., 2008, *ApJ*, submitted, arXiv:0802.0508v1 [astro-ph]
- Kang, X., & van den Bosch, F. C., 2008, *ApJ*, 676, L101
- Kassin, S. A. , Weiner, B. J. , Faber, S. M. , Koo, D. C. , Lotz, J. M. , Diemand, J. , Harker, J. J. , Bundy, K. , Metevier, A. J. , Phillips, A. C. , Cooper, M. C. , Croton, D. J. , Konidaris, N. , Noeske, K. G. and Willmer, C. N. A., 2007, *ApJ*, 660, L35
- Katz, N., 1992, *ApJSupp.*, 391, 502
- Katz, N., Quinn, T., Bertschinger, E. & Gelb, J. M., 1994, *MNRAS*, 270, L71
- Katz, N., Hernquist, L., & Weinberg, D.H., 1999, *ApJ*, 523, 463
- Kereš, D., Katz, N., Weinberg, D.H., & Dav'e, R., 2005, *MNRAS*, 363, 2
- Koda, J. Milosavljevic, M. Shapiro, P., *ApJ*, submitted, arXiv:0711.3014 [astro-ph]
- Lucy, L.B. 1977, *AJ*, 82, 1013
- Maller, A., H., Katz, N., Keres, D., Davé, R., Weinberg, D.H., 2006, *ApJ*, 647, 763
- Mathewson, D.S., Ford, V.L. & Buchorn, M., 1992, *ApJ-Supp.* 81, 413
- Mayer, L., Governato, Fabio & Kaufmann, T., 2008, *Advanced Science Letters*, in press, arXiv:0801.3845
- Meneux, B., Guzzo, L., Garilli, B., Le Fevre, O., Pollo, A., Blaizot, J., De Lucia, G., Bolzonella, M., Lamareille, F., Pozzetti, L., Cappi, A., Iovino, A., Marinoni, C., McCracken, H. J., de La Torre, S., Bottini, D., Le Brun, V., Maccagni, D., Picat, J. P., Scaramella, R.; Scodreggio, M.; Tresse, L., Vettolani, G., Zanichelli, A., Abbas, U., Adami, C., Arnouts, S., Bardelli, S., Bongiorno, A., Charlot, S., Cilieggi, P., Contini, T.; Cucciati, O., Foucaud, S., Franzetti, P., Gavignaud, I., Ilbert, O., Marano, B., Mazure, A., Merighi, R., Paltani, S., Pell, R.; Radovich, M.; Vergani, D.; Zamorani, G., & Zucca, E., 2008, *A&A*, 478,299
- Moore, B., Katz, N., Lake, G., Dressler, A. & Oemler, A., *Nature*, 379, 613
- Naab, T., Johansson, P. H., Ostriker, J. P. & Efstathiou, G., 2007, *ApJ*, 658, 710
- Navarro, J.F., 1998, preprint, astro-ph/9807084
- Navarro, J.F., and Steinmetz, M., 2000, *ApJ*, 538, 477
- Nuijten, M. J. H. M. , Simard, L. , Gwyn, S. and Röttgering, H. J. A., 2005, *ApJ*, 626, L77
- Okamoto, T., Eke, V.R., Frenk, C.S. & Jenkins, A., 2005, *MNRAS*, 363, 1299
- Okamoto, T., Nemmen, R. S., & Bower, R. G., 2007, *MNRAS*, submitted, eprint arXiv:0704.1218
- Park, C. , Choi, Y.-Y. , Vogeley, M. S. , Gott, J. R. I. , and Blanton, M. R., *ApJ*, 658, 898
- Pelupess, F.I., Papadopoulos, P. P. & van der Werf, P., 2006, *ApJ*, 645, 1024
- Peter, A. H. G. and Shapley, A. E. and Law, D. R. and Steidel, C. C. and Erb, D. K. and Reddy, N. A. and Pettini, M., 2007, *ApJ*, in press, ArXiv e-print 0706.2865
- Postman, M., Franx, M., Cross, N. J. G., Holden, B., Ford, H. C., Illingworth, G. D., Goto, T., Demarco, R., Rosati, P., Blakeslee, J. P., Tran, K.-V., Bentez, N., Clampin, M., Hartig, G. F., Homeier, N., Ardila, D. R., Bartko, F., Bouwens, R. J., Bradley, L. D., Broadhurst, T. J., Brown, R. A., Burrows, C. J., Cheng, E. S., Feldman, P. D., Golimowski, D. A., Gronwall, C., Infante, L., Kimble, R. A., Krist, J. E., Lesser, M. P., Martel, A. R., Mei, S., Menanteau, F., Meurer, G. R., Miley, G. K., Motta, V., Sirianni, M., Sparks, W. B., Tran, H. D., Tsvetanov, Z. I., White, R. L. & Zheng, W., 2005, *ApJ*623, 721
- Portinari, L., & Sommer-Larsen, J., 2007, *MNRAS*375, 913
- Price, D.J., 2007, *J. Comp. Phys* in press, eprint arXiv:0709.2772
- Robertson, B, Yoshida, N., Springel, V. and Hernquist, L., *ApJ*, 2004, 606, 32
- Saro, A., Borgani, S., Tornatore, L. , Dolag, K., Murante, G., Biviano, A., Calura, F. and Charlot, S., 2006, *MNRAS*, 373, 397
- Sersic, J.L., 1968, *Atlas de Galaxias Australes* (Cordoba: Obs. Astron.)
- Sijacki, D., Springel, V., di Matteo, T. and Hernquist, L., 2007, *MNRAS*, 380, 877
- Smith, G. P. , Treu, T. , Ellis, R. S. , Moran, S. M. and Dressler, A., 2005, *ApJ*, 620, 78
- Sommer-Larsen, J., Gotz, M., Portinari, L., 2003, *ApJ*, 596,47
- pergel03 Spergel, D. N., Verde, L., Peiris, H. V., Komatsu, E., Nolta, M. R., Bennett, C. L., Halpern, M., Hinshaw, G., Jarosik, N., Kogut, A., Limon, M., Meyer, S. S., Page, L., Tucker, G. S., Weiland, J. L., Wollack, E. & Wright, E. L., 2003, *ApJSupp.*, 148, 175
- Springel, V., Yoshida, N., & White, S.D.M. 2001, *New Astronomy*, 6, 79
- Springel, V. & Hernquist, L., 2003a, *MNRAS*, 339, 289
- Springel, V. & Hernquist, L., 2003b, *MNRAS*, 339, 312
- Springel, V., 2005, *MNRAS*, 364, 1105
- Springel, V., Di Matteo, T., and Hernquist, L., 2005, *MNRAS*, 361, 776
- Springel, V. , White, S. D. M. , Jenkins, A. , Frenk, C. S. , Yoshida, N. , Gao, L. , Navarro, J. , Thacker, R. , Croton, D. , Helly, J. , Peacock, J. A. , Cole, S. , Thomas, P. , Couchman, H. , Evrard, A. , Colberg, J. and Pearce, F., 2005, *Nature*, 435, 629
- Steinmetz, M. & Navarro, J.F., 1999, *ApJ*, 513, 555
- Treu, T., Ellis, R.S., Kneib, J.-P., Dressler, A., Smal, I., Csoos, O., Oemler, A. & Natarajan, P., 2003, *ApJ*, 591, 53
- Tully, R.B., & Fisher, J.R., 1977, *A&A* 54, 661
- van den Bosch, F. C., Abel, T., Croft, R. A. C., Hernquist, L. & White, S. D. M., 2002, *ApJ*, 576, 21
- van den Bosch, F. C., Aquino, D., Yang, X., Mo, H. J., Pasquali, A., McIntosh, D. H., Weinmann, S. M., Kang, X., 2007, *MNRAS*, submitted, eprint arXiv:0710.3164
- Weinmann, S., van den Bosch, F., Yang, X., and Mo, H, 2008, in preparation.
- Weinberg, D. H., Davé, R., Katz, N., and Hernquist, Lars, 2004, *ApJ*, 601, 1
- Zavala, J. Okamoto, T. , & Frenk, C.S., 2007, *MNRAS*submitted, arXiv:0710.2901
- Zheng, Z., Coil, A., & Zehavi, I., 2007, *ApJ*, 667, 760.